Assessing the Improvements GAIA-DR1 Will Bring to Dynamical Astronomy

Mateo Prgomet

Lund Observatory
Lund University

2017-EXA126

Degree project of 15 higher education credits
June 2017

Supervisor: David Hobbs

Lund Observatory
Box 43
SE-221 00 Lund
Sweden

Abstract

The first part of this thesis deals with the dynamical estimation of the Oort constants using proper motions and parallaxes provided from the Gaia-DR1 TGAS catalogue. The photometric information was provided by the 2MASS catalogue. The Oort constants calculated from the TGAS catalogue are compared to those obtained from the original Hipparcos catalogue in order to attempt to estimate how well Gaia-DR1 performs. A least squares approach was implemented to calculate the Oort constants. This routine contained seven parameters where the stellar LSR velocity components were included as well. The overall trend seems to be such that the TGAS catalogue can provide meaningful and potentially better results compared to that of the Hipparcos catalogue if the study is not sensitive to a catalogue that is colour incomplete. TGAS worked fairly well in the determination of the Oort constants mainly due to its large sample size, giving it a statistical edge over the Hipparcos catalogue.

In the second part of the thesis the local mass density, ρ_0, was determined using tracer star populations for two catalogues. The first one was the original Hipparcos catalogue where the data was propagated to the year 2015. The second catalogue was a combination of Hipparcos stars obtained from both the TGAS and the propagated HIP catalogues. This was done in order to avoid the incompleteness issue that resulted after the creation of the TGAS catalogue.

The estimated local mass density from the propagated Hipparcos catalogue was $\rho_0 = 0.112 \pm 0.009$ $M_\odot$ pc^{-3} while the combined TGAS sample got $\rho_0 = 0.113 \pm 0.006$ $M_\odot$ pc^{-3}. This result implies that the TGAS catalogue is slightly better compared to the HIP catalogue in performance since it provides with lower formal errors.

Based on the results of the two dynamical estimations performed, the TGAS catalogue can be seen as marginally better when compared to the HIP catalogue. In addition, the formal errors resulting from the calculations using the TGAS catalogue are better compared to those obtained using the HIP catalogue. The formal errors are especially good when dynamically estimating the Oort constants since so many stars are included in the calculations. It is, however, difficult to estimate the performance of the complete Gaia catalogue by simply considering the first data release. The release of Gaia-DR2 will hopefully resolve the questions surrounding the performance of the Gaia catalogue.

Populärvetenskaplig beskrivning

Genom att observera och intervjua invånarna i Lund, kan man erhålla mycket information om historien och infrastrukturen för staden. Detta tyder på en särskilt självklar princip; om man studerar de mindre beståndsdelarna av ett system, så kan man erhålla egenskaper som är gällande för systemet i helhet. Detta är precis vad dagens astronomer utnyttjar för att lära sig mera om vårt universum. De minsta beståndsdelarna i en galax är stjärnorna, och genom att samla information för alla dessa så kan man erhålla detaljer kring galaxens utveckling och struktur. Gaia uppdraget har precis detta i åtanke. I detta väldigt ambitiösa projekt så hoppas man kunna kartlägga Vintergatan genom att ta mätningar för ungefär en miljard stjärnor. Med denna moderna kartläggningen av galaxen så hoppas man kunna upptäcka mer om vad Vintergatan består av, dess historia och dess evolution.

Gaia lanserades 2014 och förmodas vara helt avslutad omkring 2022 och kommer då kunna erbjuda den största astrometriska stjärnkatalogen någonsin. Eftersom man inte förväntas få en komplett stjärnkatalog från Gaia förräns om ungefär 5 år, så kommer det lanseras mellanliggande, mindre kataloger som innehåller den information man lyckats samla in under tiden. Den första av dessa mindre katalogerna kallas för Gaia-DR1 (Gaia Data Release 1) och innehåller information för de första 14 månaderna som projektet varit aktivt. Det är denna mindre katalog som vi har använt i detta examensarbete i ett försök att uppskatta den totala prestandan som den kompletta Gaia katalogen kommer att erbjuda. Genom att redan nu undersöka möjligheterna och begränsningarna med Gaia, kan vi planera i förtid på hur de kommande projekten som använder sig av Gaia kommer kunna ge oss en större inblick i hur vårt universum fungerar. Astronomerna hoppas kunna erhålla den mest kompletta beskrivningen av vår galax någonsin genom implementationen av den information som Gaia kommer att erbjuda.

Contents

1 INTRODUCTION

For over nine decades astronomers have studied the distribution and kinematics of stellar objects in an attempt to uncover the history and structure of the Milky Way. Kapteyn & van Rhijn (1920) could nearly 100 years ago give estimates of the size and thickness of the galaxy using stellar data that was provided at the time. Two years later Kapteyn (1922) could provide the first reasonable estimate of the mass density for the Milky Way using radial velocity and proper motion measurements of stars in the solar neighbourhood. In Oort's pioneering paper from 1927 he pointed out that the mass of the galaxy as inferred by Kapteyn was not sufficiently large to keep the globular clusters and RR Lyrae stars bound to the galaxy, thus giving an indication of the existence of dark matter.

The great success in technological advancement during the last 30 years has allowed instrumentation to be improved leading to the possibility of more accurate measurements of positions and velocities for stellar objects. Consequently, considerable amounts of resources have previously been, and still are devoted to astrometric space missions such as the Hipparcos mission and the still very modern Gaia space mission. The Hipparcos satellite was launched in 1989 by the European Space Agency, being the first space mission with the purpose to collect astrometric data of stars in the Milky Way. It managed to pinpoint more than 100 000 stars with an accuracy that was 200 times better than any mission conducted previously. The data containing measurements of positions, distances and proper motions of stars could then be used to refine the distance scale of the galaxy. Even though the mission was limited in both size and observed volume, it still provided significant knowledge regarding the structure and dynamics of the Milky Way (Perryman 2008).

The Gaia mission was launched in 2013 with the aim to measure the spatial and velocity distributions, for an expected sample size of one billion stars, in six dimensions (positions, proper motions and radial velocities). The main goal of the Gaia mission is to explore the subjects of the formation, structure and evolution of the galaxy by the creation of a six dimensional mapping of the Milky Way. There will be a number of intermediate Gaia data releases, where the first is referred to as Gaia Data Release 1 (Gaia-DR1) and was released to the scientific community after 14 months of measurements. (Gaia Collaboration et al.: Gaia Mission 2016). However, the data provided from Gaia-DR1 is not viable for usage on its own. Instead other catalogues named Tycho-2 and Hipparcos were needed to define positions at an earlier epoch, thus giving accurate proper motions for the so called TGAS solution. This catalogue provides a five parameter astrometric solution for stars in both the Hipparcos and Tycho-2 catalogues (Michalik et al. 2014). Gaia-DR1 on its own only provides photometry in the Gaia G-band, thus the inclusion of an additional survey is necessary in order to obtain photometric information. The survey used here is called 2MASS and provides photometry for stars in the near infrared bandpasses J, H and K_s.

The purpose of this thesis is to investigate the potential improvements that the Gaia-DR1 brings to dynamical astronomy. The data used consists of both the Hipparcos catalogue and a cross-match between the TGAS & 2MASS catalogues. Initially, the values of the Oort constants A, B, C and K that describe properties of the local velocity field are dynamically estimated using proper motions and a least squares routine. The mean motion of material in the solar neightbourhood, also called the local standard of rest (LSR), was estimated by expanding the least squares routine such that it contains the LSR velocity components of the Sun, (u_0, v_0, w_0). In addition to all this, the mass density in the solar neighbourhood, ρ_0, is estimated using tracer star densities in the galactic plane.

2 DATA

2.1 The Hipparcos Catalogue

The Hipparcos catalogue was published in 1997 where it contained, in total, 118 218 stars. Out of the total sample size, approximately 99.78 percent had astrometric data for the positions, parallaxes and proper motions in the J1991.25 epoch. The data was of very high quality where the standard errors were of the order 1-1.2 mas in addition to a systematic error of ≤ 0.1 mas. For the large majority of the stars in the Hipparcos sample, photometric data in the V-band as well as values for the colour index $B-V$ were provided. These colours will be of use when the Oort constants and the local mass density are to be calculated from the stars provided in the Hipparcos catalogue. It is also worth mentioning that the catalogue is complete to $V \simeq 8.0$, which will be of particular importance when calculating ρ_0. For more information regarding the Hipparcos catalogue see Perryman et al. (1997).

2.2 Gaia-DR1 TGAS

The Gaia mission was originally proposed in 1993 by Lennart Lindegren and Michael Perryman (Gaia Collaboration, et al.: The Gaia Mission 2016). The essential goal of the mission is to clarify how the galaxy has evolved through time in a quantitative manner by the study of stellar populations confined within the Milky Way. It will provide the precision needed in order to allow evaluation of the processes surrounding the early formation of the galaxy to be explored in greater detail (Perryman et al. 2001). The mission was launched in 2013 where the nominal five year science operations phase started in the first half of 2014. The survey will be limited to a magnitude of 20.7 in the photometric G band and is expected to provide an accuracy of 24 μas on parallax measurements down to a magnitude limit of $G = 15$. At this moment, the final data products are expected to be delivered by DPAC (Data Processing and Analysis Consortium) between 2022 and 2023. Due to this long wait, it was agreed upon that the Gaia data should be released at earlier stages as intermediate data releases. The first data release is called Gaia Data Release 1 (Gaia-DR1) and contains all the data collected during the first 14 months of the operation. However, it is important to stress that the Gaia DR1 represents a preliminary release with many shortcomings and for this reason Gaia DR1 cannot be used on its own (Gaia Collaboration et al.: Gaia Data Release 1 2016). The largest issue for this study is the incompleteness of Gaia-DR1 and section 2.3 describes this in more detail.

Michalik et al. (2014) demonstrated that combining the data provided in the Hipparcos catalogue with the data from the first year of Gaia observations, a five parameter astrometric solution for all the Hipparcos stars could be obtained in what is known as the one hundered thousand proper motions project (HTPM). However, a strong limitation of the HTPM project was that the Hipparcos stars were not numerous enough in order to get a good calibration for the Gaia data. Therefore, the introduction of supplementary stars were employed, thus increasing the potential risk of biasing the HTPM data sample. However, Michalik et al. (2015) presented how this potential risk of biasing the data sample could be minimized if the auxiliary stars are replaced with those stars provided from the Tycho-2 Catalogue (Høg et al. 2000), where the positions of the Tycho-2 stars have been propagated to the Gaia epoch. The resulting catalogue of stars is called the Tycho-Gaia astrometric solution (TGAS) and gives a full sky, five parameter, unbiased astrometric solution for both Hipparcos and Tycho-2 stars. The typical standard errors for the positions and parallaxes are normally around 0.3

mas. For the Tycho-2 catalogue, the standard error in the proper motions is around 1 mas yr^{-1} while the Hipparcos catalogue provides stars that has even more precise proper motion data. Additionally to these errors, there is also a systematic parallax error of 0.3 mas. For more information regarding the accuracy of the TGAS catalogue see Gaia Collaboration et al. (2017).

2.3 Completeness of the TGAS catalogue

The Tycho-2 catalogue contains positions and proper motions for 2.5 million stars in the sky complete to 99 percent for a magnitude of $V \simeq 11.0$ (Høg et al. 2000). Hipparcos, on the other hand, provides the positions, parallaxes and proper motions for approximately 120 000 stars complete to a magnitude of around $V \simeq 8.0$ (Perryman et al. 1989). The TGAS catalogue only consists of around 2 million stars, where neither Hipparcos nor Tycho-2 are completely included in the catalogue. This in turn causes there to be a issue regarding the completeness at $V \simeq 8.0$ for the TGAS catalogue, since not all of the Hipparcos stars are included. This can be problematic when calculating the local mass density since the incompleteness may cause a drastic cut-off for the tracer stars after a certain magnitude limit. This cut-off may, in turn, cause the value of ρ_0 to become too low since the tracer population numbers might be either excluded or reduced after a certain magnitude. If possible, a correction should be implemented where the TGAS incompleteness is accounted for. It is worth mentioning that the catalogue cannot be complete to $V = 11$ (to 99 percent) unless the remaining stars from the Tycho-2 stars are added to the TGAS catalogue. However, this will still not be of great use since Tycho-2 does not provide parallax measurements (nor does it have the same quality of the data as Hipparcos), which prove to be very important when calculating stellar kinematics.

A simple correction for the incompleteness can be to exclude the Tycho-2 stars from the TGAS catalogue, and thus only use HIP stars. Combining these stars with the original Hipparcos catalogue would give a five parameter solution that is complete to $V \simeq 8.0$. By doing this, the majority of the Hipparcos stars (the ones from the TGAS catalogue) will get improved proper motion measurements while still retaining its high quality data for the remaining parameters. This should in turn give more reliable results for the local galactic density.

2.4 2MASS

Bahcall et al. (1991) pointed out at the time that the infrared part of the spectrum had not been explored in great detail even though this region is of great importance for a large number of branches within astronomy. The solution to this came in the form of the Two Micron All Sky Survey (2MASS). This project was active between 1997 to 2001 and combined the efforts of two 1.3 meter large telescopes in order to collected photometric data in the near-infrared region. The 2MASS project ended up covering 99.998 percent of the celestial sphere in the near-infrared bands J (1.25 μm), H (1.65 μm) and K_s (2.16 μm) and produced a point source catalogue consisting of almost half a billion sources. However, since this survey is ground-based, practical issues due to atmospheric effects quickly arose causing sensitivity variations as data was collected. The solution to this problem came with the introduction of magnitude limits at approximately $J = 16.0, H = 15.0$ and $K_s = 14.5$. At these magnitudes the detection of sources remains complete even under conditions where the sensitivity is at its poorest for the survey. More information regarding the 2MASS data products can be found in Cutri et

al. (2003). For details surrounding the 2MASS hardware see Skrutskie et al. (2006).

2.5 Data Cross-Match

In addition to the Hipparcos catalogue, a cross-match between the TGAS and 2MASS catalogues was also used in order to study the kinematics and distribution of stars in the galaxy. To successfully cross-match the large data sets with each other, the X-Match service provided by *Centre de Données astronomiques de Strasbourg* (CDS) was used (see Boch et al. 2016). The positional criteria on the cross-match was such that for each source in the TGAS catalogue, a source from the 2MASS catalogue is returned only if the two compared sources lie at an angular distance that is less than 0.5 arcsec from each other. The cross-match area was set such that the entire sky is considered meaning that all sources from the TGAS catalogue are cross-matched with the 2MASS catalogue. Figure 1 shows a density sky plot of the data obtained for the matched catalogue. The final cross-match product gave 2,050,000 stars with a five parameter astrometric solution for each star as well as photometric data in the G, J, H and K_s bands. Figure 2 shows all of these stars in terms of the absolute G magnitude and the $J - K_s$ colour index in a Hertsprung-Russel diagram.

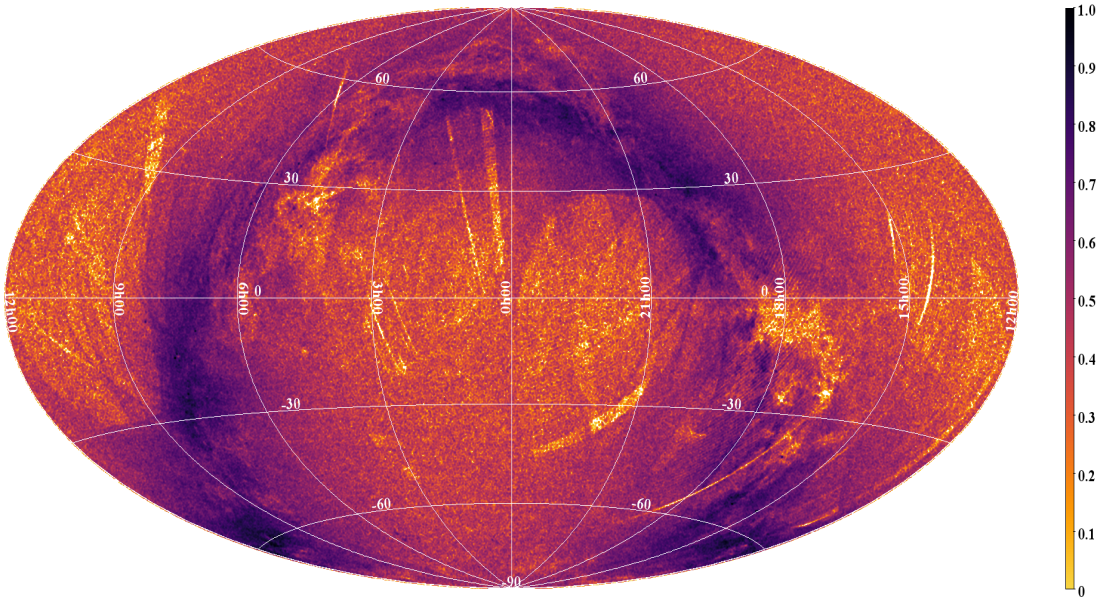

Figure 1: Density sky plot of the cross-match.

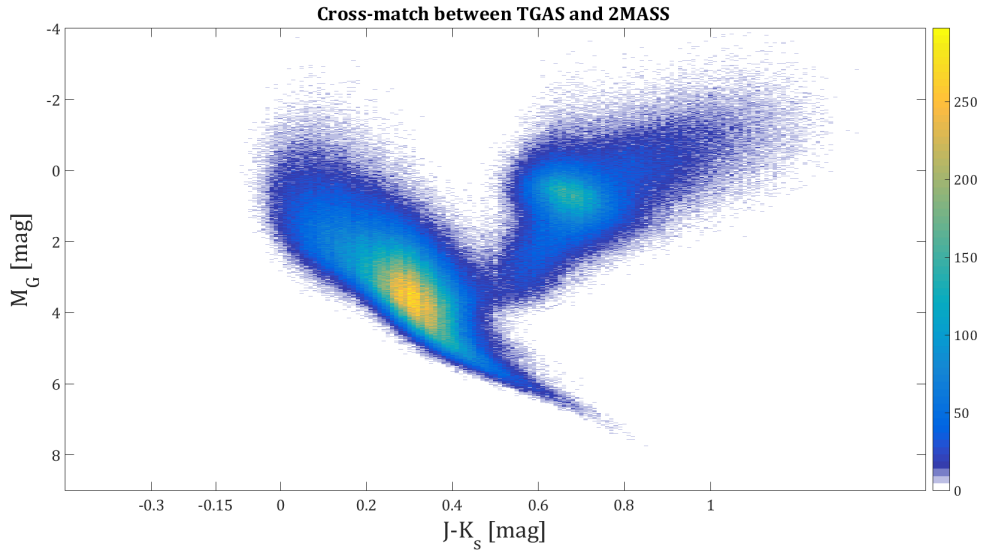

Figure 2: Hertsprung-Russel diagram of the cross-match between TGAS and 2MASS.

3 THE OORT CONSTANTS

In 1927 Oort managed to show that the motions of stars systematically vary with galactic longitude. He concluded that the reason for this is most likely due to the galaxy following differential rotation. At the time, Oort assumed the Milky Way to be axisymmetric. A consequence of this assumption is that the orbits of the stars in the galaxy are both closed and supported by the galactic gravitational potential. Thus by studying the characteristics of the galactic velocity field for an axisymmetric galaxy, properties regarding the galactic potential can be obtained. This is where the importance of the Oort constants come in. These four constants describe the velocity field of galaxies, and by determining their values, it is possible to directly infer properties of the galactic potential. However, Ogrodnikoff (1932) pointed out that the galaxy, in general, cannot be seen as axisymmetric, it is more complex than that. He shows that in addition to the streaming velocity that stars have around the galaxy, there also exists random (peculiar) velocity components. This in turn results in a more complicated relation between the velocity field and the galactic potential. The orbits of the stars for a non-axisymmetric potential cannot be seen as closed due to the existence of these random motions. Nevertheless, the calculation of the Oort constants can still provide a great deal of information regarding the galactic potential, even if there does not exist an exact relation between them.

Previously, Bobylev & Bajkova (2017) presented the values $A = -16.53 \pm 0.52\,\mathrm{km\ s^{-1}\ pc^{-1}}$ and $B = 10.82 \pm 0.93\ \mathrm{km\ s^{-1}\ pc^{-1}}$ using astrometry from Gaia-DR1 while Bovy (2016) obtained $A = 15.3 \pm 0.4\ \mathrm{km\ s^{-1}\ pc^{-1}}, B = -11.9 \pm 0.4\,\mathrm{km\ s^{-1}\ pc^{-1}}, C = -3.2 \pm 0.4\ \mathrm{km\ s^{-1}\ pc^{-1}}$ and $K = -3.3 \pm 0.6\ \mathrm{km\ s^{-1}\ pc^{-1}}$ using a cross-match between the TGAS and the APASSDR9 catalogues.

3.1 Definitions

3.1.1 The Oort Constants

The Milky Way's main motion is rotation and it can approximately be viewed as circular. Since the thickness of the galaxy is small when compared to the length, the rotation can also be seen as being confined within a thin sheet (Lindegren 2014). This rotation of the Milky Way is sometimes referred to as the streaming motion of the galaxy. In addition to the streaming velocity, stars also have a random (or peculiar) motion that can cause the streaming trajectory of the stars in the galaxy to change (Cf. Ogrodnikoff 1932). Systems where the streaming velocity dominates relative the peculiar velocity, are said to be dynamically cold. In the limit of vanishing peculiar motions (the cold limit), the streaming of the stars occur in closed orbits that are supported by the galactic gravitational potential (Olling & Dehnen 2003). Oort (1927) was the first to introduce these concepts where he considered the galaxy to follow the cold limit thus also implying that the galaxy obeys axisymmetry. Initially, We will start of by looking at the same axisymmetric galaxy that Oort did. This is, as previously mentioned, not a correct assumption but it can nevertheless give insight in the meaning of the Oort constants.

There should for every point $\boldsymbol{x}$ in the galaxy exists one average velocity, $\boldsymbol{v}$. This velocity (with unit vectors $\hat{\boldsymbol{e}}_x$ and $\hat{\boldsymbol{e}}_y$ pointing in $l = 0^\circ$ and $l = 90^\circ$ respectively) with respect to an observer at the Sun is given as

$$\boldsymbol{v} = -\boldsymbol{v}_0 + \boldsymbol{H} \cdot \boldsymbol{x} + \mathcal{O}(\boldsymbol{x}^2) \tag{1}$$

Where $\boldsymbol{v}_0$ is the solar velocity relative the local streaming motion and the matrix $\boldsymbol{H}$ is defined as

$$\boldsymbol{H} = \left[\begin{array}{cc} \partial v_x/\partial x & \partial v_x/\partial y \\ \partial v_y/\partial x & \partial v_y/\partial y \end{array} \right]_{x=0} \equiv \left[\begin{array}{cc} K+C & A-B \\ A+B & K-C \end{array} \right]$$

Where A, B, C and K are denoted as the Oort constants and describe properties of the resulting velocity field for an axisymmetric galaxy. The shear of the velocity field due to closed orbits in the azimuthal and radial direction is given by A and C respectively, the vorticity is described by B and finally the local divergence is given by the constant K (Olling & Dehnen 2003).

In two dimensional cylindrical coordinates, (R, φ), the Oort constants can be evaluated at the solar position as

$$2A = \frac{v_\varphi}{R} - \frac{\partial v_\varphi}{\partial R} - \frac{1}{R}\frac{\partial v_R}{\partial \varphi}$$

$$2B = -\frac{v_\varphi}{R} - \frac{\partial v_\varphi}{\partial R} + \frac{1}{R}\frac{\partial v_R}{\partial \varphi}$$

$$2C = -\frac{v_R}{R} + \frac{\partial v_R}{\partial R} - \frac{1}{R}\frac{\partial v_\varphi}{\partial \varphi}$$

$$2K = \frac{v_R}{R} + \frac{\partial v_R}{\partial R} + \frac{1}{R}\frac{\partial v_\varphi}{\partial \varphi}$$

It should be noted that the values of A, B, C and K described above are constant for a group of stars, but can differ when compared between stellar groups.
In the case of axisymmetry $C = K = 0$ we have

$$\frac{1}{2}\left(-\frac{v_R}{R} + \frac{\partial v_R}{\partial R} - \frac{1}{R}\frac{\partial v_\varphi}{\partial \varphi}\right) = \frac{1}{2}\left(\frac{v_R}{R} + \frac{\partial v_R}{\partial R} + \frac{1}{R}\frac{\partial v_\varphi}{\partial \varphi}\right)$$

$$\Rightarrow \frac{-2}{R}\left(v_R + \frac{\partial v_\varphi}{\partial \varphi}\right) = 0$$

$$\Rightarrow v_R + \frac{\partial v_\varphi}{\partial \varphi} = 0 \tag{2}$$

From the expression of 2C we obtain

$$2C = -\frac{1}{R}\left(v_R + \frac{\partial v_\varphi}{\partial \varphi}\right) + \frac{\partial v_R}{\partial R} = 0$$

$$\Rightarrow \frac{\partial v_R}{\partial R} = 0 \tag{3}$$

Where we utilized eq. (2) in the last step. The simplest case of differential rotation is thus given by

$$v_R \equiv 0 \quad v_\varphi \equiv v_\varphi(R) \tag{4}$$

This indicates that, for the simplest case of differential rotation, the Oort constants A and B become

$$A = \frac{1}{2}\left(\frac{v_\varphi}{R} - \frac{\partial v_\varphi}{\partial R}\right) \tag{5}$$

$$B = \frac{1}{2}\left(-\frac{v_\varphi}{R} - \frac{\partial v_\varphi}{\partial R}\right) \tag{6}$$

From these equations we obtain

$$(A-B) = \frac{v_\varphi}{R}; \quad (A+B) = -\frac{\partial v_\varphi}{\partial R}; \tag{7}$$

By measuring values of the Oort constants A and B, we can thus determine local properties of the rotation curve of the galaxy. From eq. (7) it is evident that $(A-B)$ gives the rotational velocity of the LSR around the galactic centre while $-(A+B)$ gives the slope of the rotation at the Sun's position. For additional details regarding the derivation of the expressions for the Oort constants as well as a more detailed discussion of the case $C = K = 0$ see Chandrasekhar (1960) and Lindegren (2014).

3.2 Oort Constants from Proper Motions

In the previous section we only considered the cold limit to be true for the stars in the solar neighbourhood. However, in reality the velocity field for a population of stars does vary in its divergence, vorticity and shear when compared to that of the velocity field obtained in section (3.1). Since in the cold limit the peculiar motions are vanishing, the mean streaming velocity, $\bar{\boldsymbol{v}}$, for the galaxy is equal to the closed orbit velocity, $\boldsymbol{v}$, given in eq. (1). For real galaxies however, there is normally a systematic difference between $\bar{\boldsymbol{v}}$ and $\boldsymbol{v}$ called the asymmetric drift velocity, $\boldsymbol{v}_{ad}$, given as

$$\bar{\boldsymbol{v}} = \boldsymbol{v} - \boldsymbol{v}_{ad} \tag{8}$$

Eq. (8) describes the "delay" of the mean velocity in comparison to the velocity for the local closed orbits. Due to the asymmetric drift velocity being present in most star populations, we cannot determine the Oort constants A, B, C or K since these are given only when the cold limit is valid. However, the values of $\bar{A}, \bar{B}, \bar{C}$ and $\bar{K}$ represent the Oort constants when the asymmetric drift velocity is considered. They describe properties of the real streaming velocity field *for a group of stars*. It is thus these constants that are to be determined in the case of the cold limit not being an optimal approximation. By correcting A, B, C and K for $\boldsymbol{v}_{ad}$ we have

$$\bar{A} = A - A_{ad} \tag{9a}$$

$$\bar{B} = B - B_{ad} \tag{9b}$$

$$\bar{C} = C - C_{ad} \tag{9c}$$

$$\bar{K} = K - K_{ad} \tag{9d}$$

In practice we wish to obtain values for $\bar{A}, \bar{B}, \bar{C}$ and $\bar{K}$ but might in reality not do so since the relation between the Oort constants and the average streaming velocity field can be complex. Instead we rely on proper motion data to give us values for $\tilde{A}, \tilde{B}, \tilde{C}$ and $\tilde{K}$. These are Fourier coefficients of the average proper motions for stars that are located at the same distance

$$\bar{\mu}_{l*} = \mu_u \sin l - \mu_v \cos l + \cos b[\tilde{A} \cos 2l - \tilde{C} \sin 2l + \tilde{B}] \tag{9}$$

$$\bar{\mu}_b = \sin b[\mu_u \cos l + \mu_v \sin l] - \mu_w \cos b - \sin b \cos b[\tilde{A} \sin 2l + \tilde{C} \cos 2l + \tilde{K}] \tag{10}$$

Where l denotes galactic longitude, b is the galactic latitude and the proper motion of the sun with respect to the local streaming, $\mu_\odot$, is given by

$$\boldsymbol{\mu}_\odot \equiv (\mu_u, \mu_v, \mu_w) \equiv p\boldsymbol{v}_\odot = p(u_0, v_0, w_0). \tag{11}$$

where p denotes parallax. From eq. (11) we have that $\mu_u = pv_0$, $\mu_v = pv_0$ and $\mu_w = pw_0$. Inserting this into eq. (9) and (10) we get

$$\mu_{l*} = [\tilde{A} \cos 2l - \tilde{C} \sin 2l + \tilde{B}] \cos b + p[u_0 \sin l - v_0 \cos l] \tag{12}$$

$$\mu_b = -[\tilde{A} \sin 2l + \tilde{C} \cos 2l + \tilde{K}] \sin b \cos b + p\left[(u_0 \cos l + v_0 \sin l) \sin b - w_0 \cos b\right] \tag{13}$$

It should be noted that in eqs. (12) and (13), $\tilde{A}, \tilde{B}, \tilde{C}$, and $\tilde{K}$ are, strictly speaking, not the same as $\bar{A}, \bar{B}, \bar{C}$ and $\bar{K}$. We can only measure the constants presented in eqs. (12) and (13) and hopefully the Oort constants with a bar are not too different from those with the tilde. Table 1 summarizes the different versions of the Oort constants.

Table 1:
THE OORT CONSTANTS.

Oort constants	Description
A,B,C,K	The true Oort constants obtained for the hypothetical velocity field $\boldsymbol{v}$ that is a result of the cold limit being applied (leading to closed orbits).
$\bar{A}, \bar{B}, \bar{C}, \bar{K}$	Oort constants for the resulting velocity field $\boldsymbol{v}$ when the asymmetric drift is considered for a group of stars. These are the desired constants to obtain.
$\tilde{A}, \tilde{B}, \tilde{C}, \tilde{K}$	Fourier coefficients of proper motions for a group of stars obtained from eqs. (12) and (13). This is what we can measure in practice.

For more details on how the Oort constants can be approximated using proper motions, see Olling & Dehnen (2003).

3.3 Least Squares Routine

In order to obtain values for both the Oort constants as well as the Sun's LSR velocity components, a seven variable least squares (LS) routine was employed onto the proper motion data. The details of this routine is presented below. Note that the same principles presented can be used in order to instead perform a four variable LS-routine where only the Oort constants are determined. The values of the stellar LSR velocity should then instead be held at a constant value of $(u_0, v_0, w_0) = (11.1, 12.24, 7.25)$ km/s (Schönrich et al. 2009). Only the seven variable LS routine will be presented here, but the four variable solution was implemented and results of both the routines are presented in section 3.4.

The proper motions given in eqs. (12) and (13) are the ones used to infer values of A, B, C, K, u_0, v_0 and w_0. We introduce the $7 \times n$ matrices $\tilde{\alpha}_l$ and $\tilde{\alpha}_b$ that describe the seven partial derivatives of μ_{l*} and μ_b with respect to A, B, C, K, u_0, v_0 and w_0 for a sample of n stars, respectively

$$\tilde{\alpha}_l = \begin{bmatrix} \left(\frac{\partial \mu_{l*}}{\partial A}\right)_{s_1} & \left(\frac{\partial \mu_{l*}}{\partial B}\right)_{s_1} & \left(\frac{\partial \mu_{l*}}{\partial C}\right)_{s_1} & \left(\frac{\partial \mu_{l*}}{\partial K}\right)_{s_1} & \left(\frac{\partial \mu_{l*}}{\partial u_0}\right)_{s_1} & \left(\frac{\partial \mu_{l*}}{\partial v_0}\right)_{s_1} & \left(\frac{\partial \mu_{l*}}{\partial w_0}\right)_{s_1} \\ \vdots & \vdots & \vdots & \vdots & \vdots & \vdots & \vdots \\ \left(\frac{\partial \mu_{l*}}{\partial A}\right)_{s_n} & \left(\frac{\partial \mu_{l*}}{\partial B}\right)_{s_n} & \left(\frac{\partial \mu_{l*}}{\partial C}\right)_{s_n} & \left(\frac{\partial \mu_{l*}}{\partial K}\right)_{s_n} & \left(\frac{\partial \mu_{l*}}{\partial u_0}\right)_{s_n} & \left(\frac{\partial \mu_{l*}}{\partial v_0}\right)_{s_n} & \left(\frac{\partial \mu_{l*}}{\partial w_0}\right)_{s_n} \end{bmatrix}$$

$$\tilde{\alpha}_b = \begin{bmatrix} \left(\frac{\partial \mu_b}{\partial A}\right)_{s_1} & \left(\frac{\partial \mu_b}{\partial B}\right)_{s_1} & \left(\frac{\partial \mu_b}{\partial C}\right)_{s_1} & \left(\frac{\partial \mu_b}{\partial K}\right)_{s_1} & \left(\frac{\partial \mu_b}{\partial u_0}\right)_{s_1} & \left(\frac{\partial \mu_b}{\partial v_0}\right)_{s_1} & \left(\frac{\partial \mu_b}{\partial w_0}\right)_{s_1} \\ \vdots & \vdots & \vdots & \vdots & \vdots & \vdots & \vdots \\ \left(\frac{\partial \mu_b}{\partial A}\right)_{s_n} & \left(\frac{\partial \mu_b}{\partial B}\right)_{s_n} & \left(\frac{\partial \mu_b}{\partial C}\right)_{s_n} & \left(\frac{\partial \mu_b}{\partial K}\right)_{s_n} & \left(\frac{\partial \mu_b}{\partial u_0}\right)_{s_n} & \left(\frac{\partial \mu_b}{\partial v_0}\right)_{s_n} & \left(\frac{\partial \mu_b}{\partial w_0}\right)_{s_n} \end{bmatrix}$$

Where s_1 denotes the first star and s_n the n:th star in the sample. Furthermore, we introduce the $1 \times n$ matrix that holds the proper motions in latitude and longitude respectively as

$$\tilde{\beta}_l = \begin{bmatrix} (\mu_{l*})_{s_1} \\ \vdots \\ (\mu_{l*})_{s_n} \end{bmatrix} \qquad \tilde{\beta}_b = \begin{bmatrix} (\mu_b)_{s_1} \\ \vdots \\ (\mu_b)_{s_n} \end{bmatrix}$$

Where s_1 once again denotes the first star and s_n the last in the sample. An equation of the form $\alpha^T \alpha x = \alpha^T \beta$ can generally be solved for x as

$$x = [\alpha^T \alpha]^{-1} \alpha^T \beta \tag{14}$$

Where we in this case have

$$\alpha = \begin{bmatrix} \tilde{\alpha}_l \\ \tilde{\alpha}_b \end{bmatrix} \qquad \beta = \begin{bmatrix} \tilde{\beta}_l \\ \tilde{\beta}_b \end{bmatrix} \qquad x = \begin{bmatrix} A \\ B \\ C \\ K \\ u_0 \\ v_0 \\ w_0 \end{bmatrix}$$

By solving for x we obtain the values of the Oort constants as well as values for the solar LSR velocity with respect to the stellar population. As previously mentioned, the principles of the LS solution presented above can be used in order to instead solve a four parameter LS routine. For this routine to work, the stellar LSR velocity must be held constant and the matrices $\tilde{\alpha}_l, \tilde{\alpha}_b$ and x must naturally also be adjusted to consider the four parameters A, B, C and K only.

For the seven variable LS-routine described above, it is assumed that each measurement of the proper motion for a data set provides information in an equally precise manner. In other words, each observation is treated equally. Clearly, this is not an ideal situation since there are many processes that can contribute to the worsening of a measurement. In order to compensate for this, one must reduce the effect that a measurement of lower quality has on the overall solution. It is, however, important to not simply discard the measurement since it can still contribute statistically to the study. The best way to go about this problem is to introduce weighting to the solution. Generally, a non-weighted LS-solution yields

$$\alpha^T \alpha x = \alpha^T \beta \tag{15}$$

where a solution for the matrix x can be obtained as shown previously. However, for a weighted LS-solution we instead have

$$\alpha^T W \alpha x = \alpha^T W \beta \tag{16}$$

This equation can still be solved in the same manner as described above, but with the introduction of the diagonal weight matrix W, it is possible to reduce the negative effect that lower quality data can have on the solution. The weight matrix contains the statistical weight factors, W_l, that are given as

$$W_l = \frac{w_l}{\sigma_l^2} \tag{17}$$

where σ_l represents the uncertainty of the measurement and w_l is the downweighting factor given by

$$w_l = w\left(\frac{R_l}{\sigma_l}\right) \tag{18}$$

w is a function that ranges between zero and one, where a good measurement will have $w = 1$ while lesser quality data will have values closer to zero. R_l describes the residuals. For an expression of w which is designed to remove outliers for a data sample, see eq. (66) in Lindegren et al. (2012). By the implementation of the weighting matrix W into the LS-solution as seen in eq. (16), it is possible to minimize the negative effects that low quality data can potentially have on the least squares solution. However, weighting of the data was not implemented here.

For a more detailed method on how weighting can be implemented for an LS-routine, see Lindegren et al. (2012).

3.4 Data

The selection criteria that were applied onto the Hipparcos and cross-matched catalogues are motivated in the following section and are summarized in tables 2 and 3 respectively.

3.4.1 Sample Criteria

As mentioned previously, the Oort constants can vary for different star populations. In order to get accurate results that are representative of a statistical population, it is important that the stars in the sample used for the calculations are similar in their characteristics (Lindegren 2014). For this reason, only the main sequence stars from both the catalogues (Hipparcos & matched data) were employed since they are generally more well-behaved when compared to stars in the giant branch. There are, in particular, two reasons as to why the main sequence stars are preferred over giant branch stars. Firstly, the bluer main sequence stars usually have lower velocity dispersions due to their young ages. Secondly, it is easier to identify the main sequence stars in an Hertsprung-Russel Diagram, making the data selection process less prone to contamination of stars from different populations. Figure 3 marks the main sequence in the Hertsprung-Russel diagram of the stars obtained from the complete cross-match between TGAS and 2MASS. From the main sequence stars, only those with parallaxes > 1 mas were considered in order to ensure a local sample. In addition, the fractional parallax error, σ_p/p, was not allowed to be larger than 20 percent of p. For stars that have $\sigma_p/p > 0.2$, it becomes more problematic to estimate the distance from the parallax measurement since $1/p$ can no longer be considered a good distance estimator (Bailer-Jones 2015). The maximum allowed parallax error, σ_p, was also set to be 1 mas in order to not include stars with too large errors in the study. To maximize the number of stars considered in the calculation, there were no restraints on the allowed value for the galactic latitude. For the stars following these criteria, the proper motions were converted from the equatorial coordinate system into the galactic system using the mathematical formulae derived in Poleski (2013). The proper motions were converted from [mas yr^{-1}] to [km s^{-1} kpc^{-1}] using the conversion factor $K = 4.7405$.

In order to limit the spread in age for the main sequence stars, the data was divided into three smaller bins for both the catalogues. For Hipparcos the total range in the colour index was $-0.15 < B - V \leq 0.4$ while it for the matched data was $-0.15 < J - K_s \leq 0.4$. The maximum value of the colour indices was set to 0.4 mainly due to two reasons. Firstly, for larger values of the colour index, the main sequence becomes less distinguishable from the giant branch. Including this region thus risks to contaminate the data sample with non-main sequence stars. Secondly, the age of stars increases with larger values of $J - K_s$ and $B - V$. Older stars have larger velocity dispersions and thus their streaming motions become less clear, making them more unsuitable to use in the determination of the Oort constants (Casagrande et al. 2011).

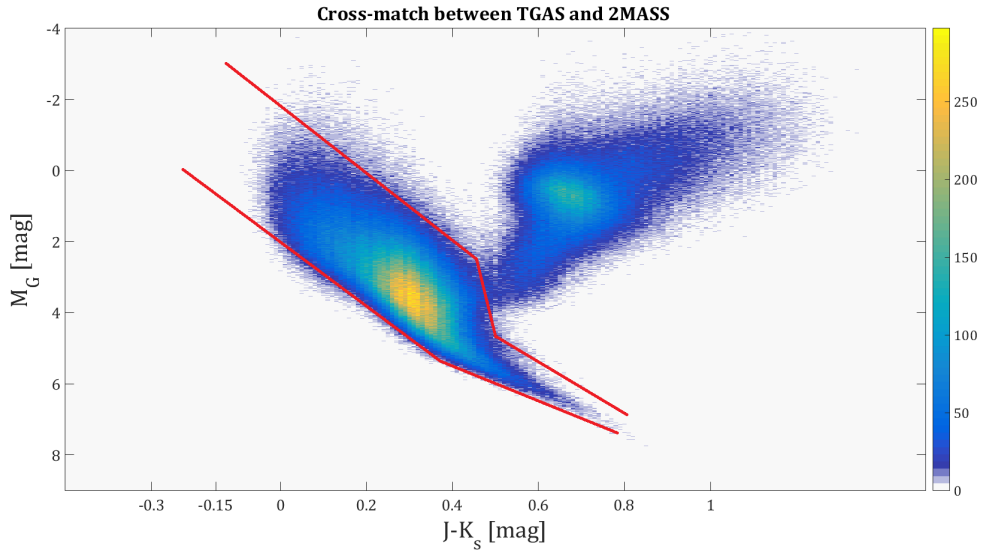

Figure 3: MAIN SEQUENCE FOR THE CROSS-MATCH BETWEEN TGAS AND 2MASS.

Table 2:
SUMMARY OF SELECTION CRITERIA FOR CROSS-MATCHED SAMPLE.

Region	p [mas]	σ_p/p	σ_p [mas]	Sample Size [stars]
$-0.15 < J-K_s \leq 0.0$	> 1.0	≤ 0.2	≤ 1.0	6281
$0.0 < J-K_s \leq 0.2$	> 1.0	≤ 0.2	≤ 1.0	99894
$0.2 < J-K_s \leq 0.4$	> 1.0	≤ 0.2	≤ 1.0	579792

Table 3:
SELECTION CRITERIA FOR THE HIP DATA SAMPLES.

Region	p [mas]	σ_p/p	σ_p [mas]	Sample Size [stars]
$-0.15 < B-V \leq 0.0$	> 1.0	≤ 0.2	≤ 1.0	1867
$0.0 < B-V \leq 0.2$	> 1.0	≤ 0.2	≤ 1.0	3869
$0.2 < B-V \leq 0.4$	> 1.0	≤ 0.2	≤ 1.0	4410

3.5 Results

Here the results of the calculations performed for the samples in tables 2 and 3 are presented. The unit of the Oort constants (described by *Value* in the tables) is $\mathrm{km\ s^{-1}\ pc^{-1}}$ while σ denotes the standard errors of the calculations and were estimated as the square root of the values of the diagonal for the respective covariance matrix.

3.5.1 Hipparcos catalogue

Tables 4 and 5 shows the results of the four and seven parameter LS-routines that were performed for the Hipparcos data samples respectively. The assumed stellar LSR velocity was $(u_0, v_0, w_0) = (11.1, 12.24, 7.25)\,\mathrm{km\ s^{-1}}$.

Table 4:
RESULTS OF THE 4 PARAMETER LS-ROUTINE FOR HIP CATALOGUE.

	$-0.15 < B-V \leq 0.0$		$0.0 < B-V \leq 0.2$		$0.2 < B-V \leq 0.4$	
	Value	σ	*Value*	σ	*Value*	σ
A	14.50	4.06	14.25	3.59	30.77	5.40
B	-19.06	3.12	-11.36	2.74	1.48	4.22
C	-19.25	4.04	-14.53	3.49	-5.39	5.20
K	-32.33	8.92	-3.34	6.92	18.36	9.19

Table 5:
RESULTS OF THE 7 PARAMETER LS-ROUTINE FOR THE HIP CATALOGUE.

	$-0.15 < B-V \leq 0.0$		$0.0 < B-V \leq 0.2$		$0.2 < B-V \leq 0.4$	
	Value	σ	*Value*	σ	*Value*	σ
A	8.65	2.68	12.53	2.96	27.59	4.58
B	-10.90	2.07	-14.31	2.27	-3.19	3.58
C	-4.89	2.68	-16.10	2.89	-6.07	4.41
K	-12.16	5.94	-10.12	5.73	12.54	7.79
u_0	12.50	0.26	8.67	0.23	12.44	0.28
v_0	13.69	0.30	9.20	0.24	8.72	0.30
w_0	7.58	0.25	6.56	0.24	6.51	0.27

If for the Hipparcos catalogue the fractional parallax errors were increased, the results of the calculations did not provide with more meaningful results other than a reduction of the standard errors. This is due to the size of the samples presented in table 3 becoming larger.

However, the data considered when $\sigma_p/p > 0.2$ is applied is not of high quality and in return causes a reduction in reliability of the results, regardless of the decreased standard errors. Figures 4-6 show plots of the residuals, $\Delta\mu_{l*} = (\mu_{l*} - p(u_0 \sin l + v_0 \cos l))$ versus galactic longitude for the three sub-samples respectively. The blue line corresponds to the mean given as $(A \cos 2l - C \cos 2l + B) \cos(b)$. The scatter of the stars in the figures is farily large, thus increasing the difficulty in verifying if the fit of the mean equation onto the data is good. Additional figures can be found in Appendix A.

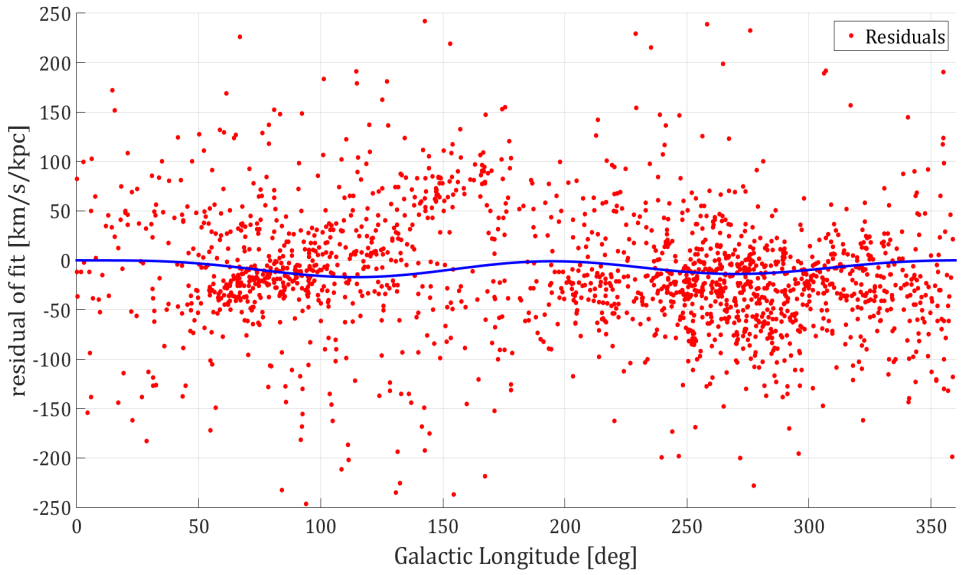

Figure 4: $\Delta\mu_{l*}$ VS. l FOR THE HIP SAMPLE THAT RANGES BETWEEN $-0.15 < B - V \leq 0.0$.

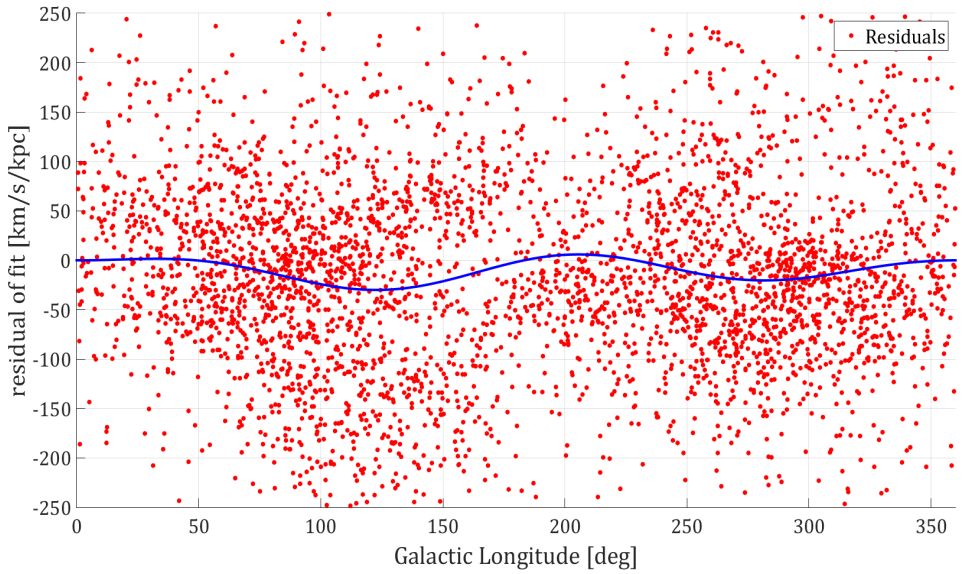

Figure 5: $\Delta\mu_{l*}$ VS l FOR THE HIP SAMPLE IN THE REGION $0.0 < B - V \leq 0.2$.

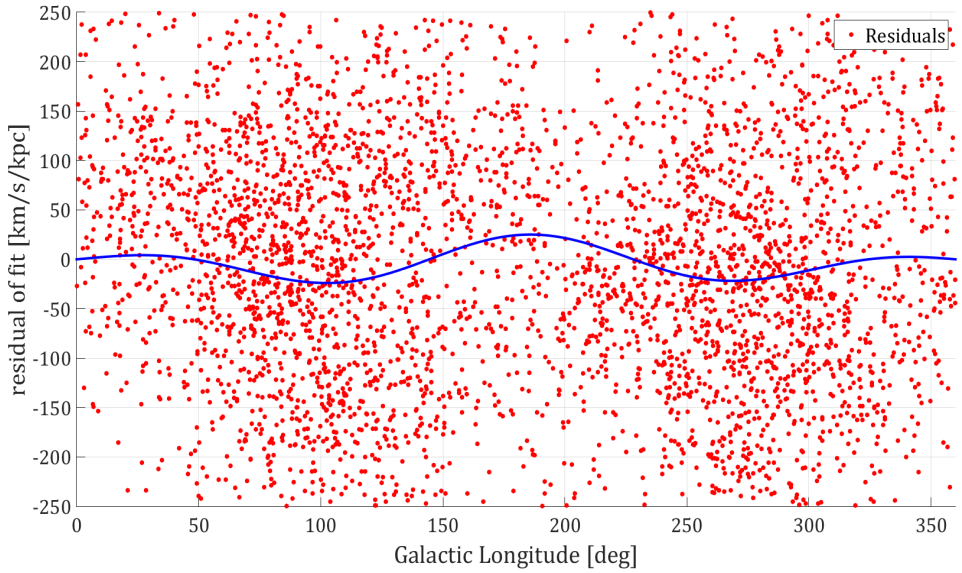

Figure 6: $\Delta\mu_{l*}$ VS. l FOR THE THIRD HIP SAMPLE RANGING BETWEEN $0.2 < B-V \leq 0.4$.

3.5.2 TGAS & 2MASS cross-match

Table 6 shows the calculated Oort constants for the four parameter LS-routine where the stellar LSR velocity was once again held constant at $(u_0, v_0, w_0) = (11.1, 12.24, 7.25)$ km/s. Table 7 contains the results of the seven parameter least square routine. The unit for the Oort constants is km s^{-1} pc^{-1}.

Table 6:
RESULTS OF THE 4 PARAMETER LS-ROUTINE FOR THE CROSS-MATCH.

	$-0.15 < J-K_s \leq 0.0$		$0.0 < J-K_s \leq 0.2$		$0.2 < J-K_s \leq 0.4$	
	Value	σ	*Value*	σ	*Value*	σ
A	18.91	1.22	16.61	0.32	17.30	0.25
B	-7.03	0.93	-10.43	0.24	-9.81	0.19
C	-0.25	1.25	-5.21	0.32	-4.11	0.24
K	-16.56	3.51	-2.28	0.83	-5.36	0.48

Table 7:
RESULTS OF THE 7 PARAMETER LS-ROUTINE FOR THE CROSS-MATCH.

	$-0.15 < J - K_s \leq 0.0$		$0.0 < J - K_s \leq 0.2$		$0.2 < J - K_s \leq 0.4$	
	Value	σ	*Value*	σ	*Value*	σ
A	9.45	1.07	13.91	0.30	16.53	0.22
B	-15.36	0.81	-13.10	0.22	-12.09	0.17
C	-1.17	1.07	-5.17	0.30	-3.04	0.22
K	-7.17	3.02	-2.81	0.77	-4.30	0.43
u_0	6.51	0.21	6.86	0.07	8.80	0.04
v_0	13.95	0.24	9.22	0.08	18.02	0.04
w_0	5.93	0.19	6.11	0.06	7.05	0.04

The values of the Oort constants presented in table 6 differ quite significantly from those in table 7. In addition, the stellar LSR velocities (u_0, v_0, w_0) from table 7 do not agree very well with those provided by Schönrich et al. (2009). The discrepancies for the calculated values might be due to correlation between the parameters. To investigate this further, a correlation analysis was performed for the Oort constants as well as the LSR velocity components. The average Pearson correlation coefficients between the three data bins are presented in table 8. The variable pairs that have a Pearson correlation coefficient larger than 0.04 (corresponding to a 4 percent correlation) are marked in red. It is evident from table 8 that there is indeed a linear correlation between some of the velocities (u_0, v_0, w_0) and the Oort constants (A, B, C, K). In particular, the Oort constants A and B show a fairly strong correlation towards the LSR velocity component v_0. There is also correlation between the Oort constants themselves. This is, however, to be expected since they all describe properties of the local velocity field.

Figures 7-9 shows the residuals of the proper motion in galactic longitude, $\Delta\mu_{l*} = (\mu_{l*} - p(u_0 \sin l + v_0 \cos l))$, for the three sub-samples from the cross-matched TGAS catalogue. The blue line once again represents the mean given by $(A \cos 2l - C \cos 2l + B) \cos(b)$. It is considerably easier to verify that the mean equation is a fairly good fit for the data from figures 7-9 compared to those provided for the Hipparcos catalogue, meaning that the differential rotation of the galaxy can be inferred from the values of the Oort constants. See Appendix A for more figures.

Table 8:
PEARSON CORRELATION COEFFICIENTS BETWEEN VARIABLE PAIRS.

	A	B	C	K	u	v	w	
A	1.000	0.239	-0.019	-0.008	0.037	-0.102	-0.011	A
B	0.239	1.000	0.025	-0.007	0.002	-0.104	-0.010	B
C	-0.019	0.025	1.000	-0.026	-0.028	0.038	0.000	C
K	-0.008	-0.007	-0.026	1.000	-0.022	-0.023	0.021	K
u	0.037	0.002	-0.028	-0.022	1.000	0.014	-0.003	u
v	-0.102	-0.104	0.038	0.023	0.014	1.000	0.064	v
w	-0.012	-0.010	0.000	0.021	-0.003	0.064	1.000	w
	A	B	C	K	u	v	w	

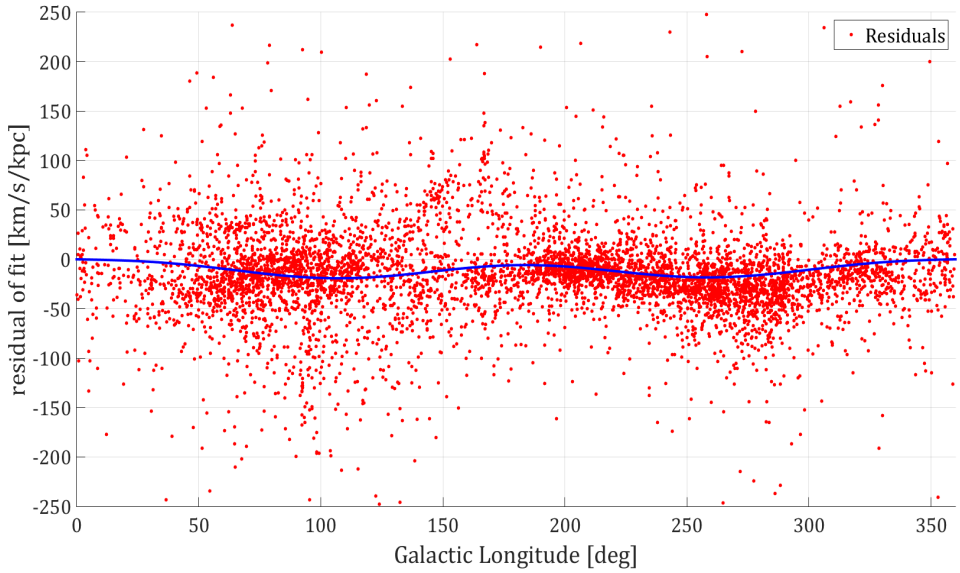

Figure 7: $\Delta\mu_{l*}$ VS. LONGITUDE FOR THE MATCHED SAMPLE WITHIN $-0.15 < J - K_s \leq 0.0$.

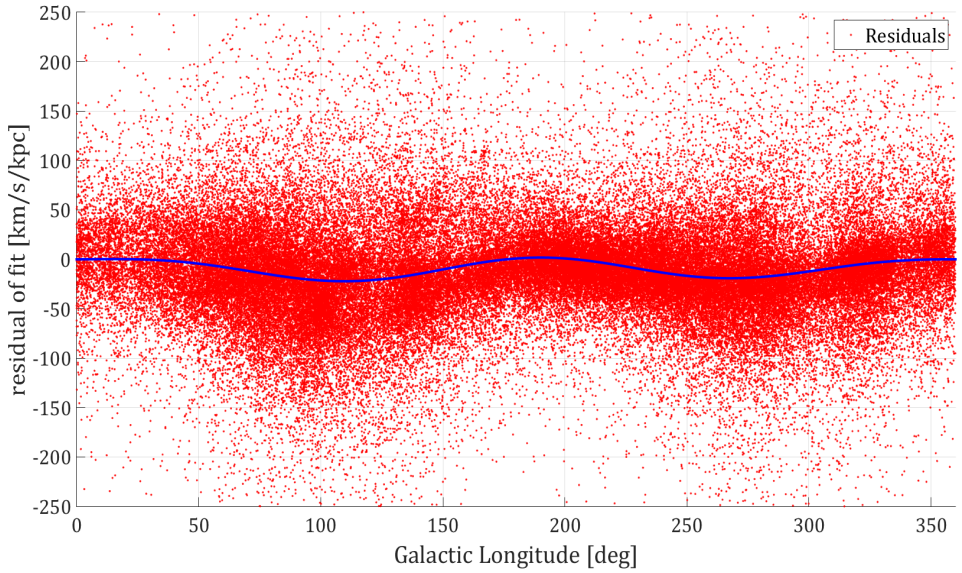

Figure 8: $\Delta\mu_{l*}$ FOR THE SECOND MATCHED SUB-SAMPLE RANGING BETWEEN $0.0 < J - K_s \leq 0.2$.

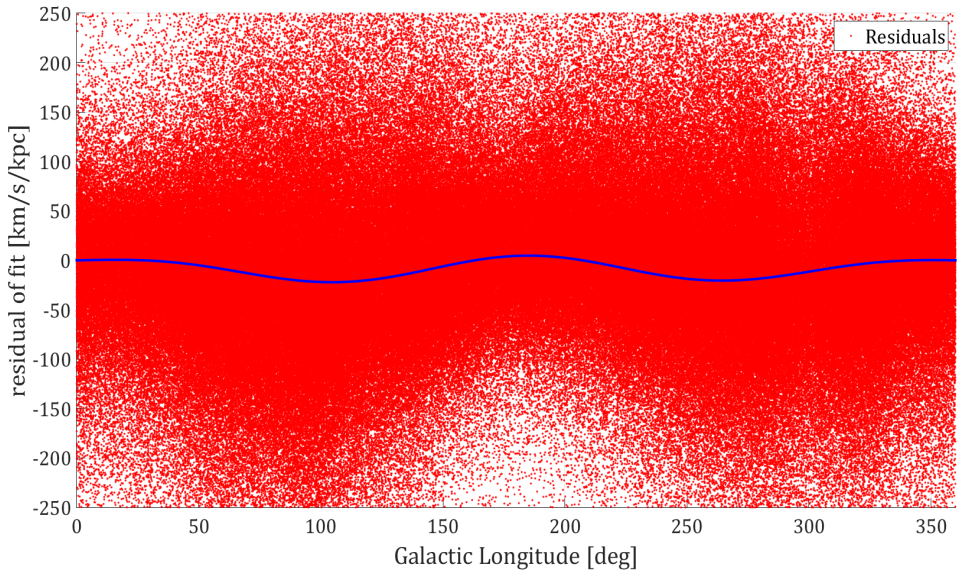

Figure 9: $\Delta\mu_{l*}$ FOR THE LARGEST CROSS-MATCH SAMPLE RANGING BETWEEN $0.2 < J - K_s \leq 0.4$.

3.6 Conclusion

The results presented in tables 4 and 5 show values of the Oort constants that are significantly different between the three samples defined by the range in colour index. This spread is most likely due to the number of stars per sample being low. However, the third sample of the Hipparcos catalogue that ranged between $0.2 < B - V \leq 0.4$ contained the most stars compared to the other sub-samples. Despite this, the values of A, B, C and K from both the four and seven parameter LS routines, were not in very good agreement with literature values. This is an indication that sample size is an important factor when calculating values of the Oort constants.

The results from the matched data between the TGAS and 2MASS catalogues show significant improvement when looking at the spread of the calculated Oort constants for the three regions in the colour index. The formal errors are also considerably smaller when compared to those provided by the Hipparcos catalogue. This should most likely be due to the sample size of the matched data being significantly larger compared to the original HIP catalogue, thus a drastic improvement in the statistical aspect of the study could be expected.

The sample that ranged between $0.2 < J - K_s \leq 0.4$ contained a very large amount of stars that were located towards the end of the main sequence, thus increasing the risk of contamination from the giant branch. Excluding the possibility of correlation, this might be the reason as to why there is a slight difference between the results for the four and seven parameter LS routines. In the second sample that ranged between $0.0 < J - K_s \leq 0.2$, the stars were concentrated more towards the main sequence and away from the giant branch. The stars in this sample are thus most likely not suffering from a contamination that is as severe when comparing to that of the previously discussed sample. The good results from both the LS routines for this sample could then be a direct result of the balance between low contamination of giant branch stars as well as sample size being sufficiently large. The first sample does not provide very good results mainly due to its very small size. Overall, the TGAS catalogue could provide with values of the Oort constants that were in fairly good agreement with those presented by Bovy (2016), and judging by the results presented, the TGAS catalogue does work slightly better than the Hipparcos catalogue. However, it is important to note that the methods used in this thesis to calculate the Oort constants did not include weighting of the data. This might potentially be a large improvement of the study and could eventually provide results that are different from those provided here. Since the TGAS catalogue contains many stars, it can still provide with results from a statistical point of view, while the Hipparcos catalogue is considerably weaker in this regard due to its sample size. This is evident from tables 4-7 where the results provided by the Hipparcos catalogue are more inconsistent between the samples compared to that of the matched data. It should, however, be noted that the Hipparcos stars contained within the TGAS catalogue are those that have the largest impact due to their high quality data. For this reason, the inclusion of weighting to the study could potentially improve the results obtained from the Hipparcos catalogue.

In conclusion, the TGAS catalogue can provide meaningful results and statistical improvements to studies that are not compromised by the colour incompleteness of the catalogue, such as the determination of the Oort constants. The results are more statistically complete when compared to those obtained from the HIP catalogue, but since weighting is not included here, it is difficult to convey if the performance of the TGAS catalogue is decisively better than that of the Hipparcos catalogue. Based on the results without the inclusion of weighting, the

TGAS catalogue seems to perform slightly better than the Hipparcos catalogue. However, the questions regarding what catalogue is more optimal for a study like this, will most likely be resolved when Gaia-DR2 is presented, and the data from the Gaia mission can be used more directly to determine galactic properties.

4 LOCAL MASS DENSITY ESTIMATION

In this section the local mass density is dynamically estimated using the motions and number density profiles of tracer star populations. The data consists of only Hipparcos stars from both the original HIP catalogue propagated to the year 2015 as well as those provided in the Gaia DR1 TGAS catalogue. Previous studies regarding the local mass density took advantage of the high quality astrometric data provided by Hipparcos. Créze et al. (1998) obtained a value of $\rho_0 = 0.076 \pm 0.015\ M_\odot\ \mathrm{pc}^{-3}$ while Holmberg & Flynn (2000) instead procured a value $\rho_0 = 0.102 \pm 0.010\ M_\odot\ \mathrm{pc}^{-3}$, where both studies used Hipparcos data. Historically, the determination of the local mass density has been an interesting topic for astronomers. Oort (1932) was the first to determine a value of ρ_0, with many astronomers quickly following his direction. Kerr & Lunden-Bell (1986) provides a short summary of all the calculated values of ρ_0 between 1932 and 1984. Comparing the values for the local mass density provided by Créze et al. and Holmberg & Flynn with those provided in Kerr & Lunden-Bell, there is a slight difference. The overall trend indicates that the more modern calculations of the mass density in the solar neighbourhood yield slightly lower values than what was previously expected. When the Gaia data is fully released the questions regarding the value of the local mass density will hopefully be given a definitive answer. By implementing the Hipparcos stars from the TGAS catalogue in the determination of ρ_0, a first indication on how the complete Gaia catalogue will perform, might be obtained.

4.1 Definitions

4.1.1 Galactic Plane Density

In what follows, an expression for the local mass density, ρ_0, will be derived using the principles described in Lindegren (2014).

By studying the motions of a collection of stars in a gravitational field, it is possible to estimate the density of the star population. These motions are described by the Jeans equations. However, motions of disk stars in the solar neighbourhood can be seen as varying in only the z-direction normal to the galactic plane. This is an approximation that works rather well for stars in the solar neighbourhood since the thickness of the galactic disk is considerably smaller in comparison to the scale length. So, in short, by looking at how the motions in a population of stars vary in the z-direction due to gravity, one can to a good approximation, say something about the density for that population.

By using the third Jeans equation and only considering star motions in the z-direction we obtain

$$-\frac{\partial \psi}{\partial z} = \langle w \rangle \frac{\partial \langle w \rangle}{\partial z} + \frac{1}{n}\frac{\partial (n D_{ww})}{\partial z} \tag{19}$$

The left hand side of eq. (19) is the force in the z-direction. The right hand side contains the average velocity in the z-direction, $\langle w \rangle$, the tracer star density, $n(z)$ and the velocity dispersion in the z-direction, $D_{ww} = \sigma_w^2$. Due to symmetry, there should be no net motion of stars in either z-direction through the galactic plane and thus $\langle w \rangle = 0$. We can then simplify eq. (19) even further by simply removing the term that contains $\langle w \rangle$, replacing D_{ww} with σ_w^2 and noting that the partial derivative can be written as

$$\frac{1}{n(z)}\frac{\partial n(z)}{\partial z} = \frac{\partial \ln n(z)}{\partial z}$$

The resulting version of eq. (19) then becomes

$$\frac{\partial \psi}{\partial z} = -\sigma_w^2 \frac{\partial \ln n(z)}{\partial z} \tag{20}$$

Where $\partial\psi/\partial z$ is commonly referred to as K_z and describes the vertical force applied on all the stars in the population. Note that eq. (20) is only valid for all stars in a population if σ_w is independent of z i.e. it needs to be constant for a population of stars.
If we take the partial derivative of K_z with respect to z it can be put equal to the Poisson equation, thus giving

$$\frac{\partial K_z}{\partial z} = -\sigma_w^2 \frac{\partial^2 \ln n(z)}{\partial z^2} = 4\pi G \rho(z) \tag{21}$$

From this it is possible to obtain the galactic plane density as

$$\rho_0 = \rho(0) = -\frac{\sigma_w^2}{4\pi G} \left[\frac{\partial^2 \ln n(z)}{\partial z^2} \right]_{z=0} \tag{22}$$

Note that in order to obtain a value for σ_w^2, the dispersion matrix is needed. The details surrounding its estimation can be found in Appendix B.

4.2 Data

As mentioned in section 2.3, in order to calculate the local mass density, a catalogue that is complete to a certain magnitude is necessary. However, in the creation of the TGAS catalogue, only a fraction of the Hipparcos catalogue as well as a fraction of the Tycho-2 catalogue were included. This in turn caused there to be an incompleteness issue of the TGAS catalogue, and it cannot be used directly to determine the local mass density. Instead a correction must be implemented. The Hipparcos stars in the TGAS sample were manually extracted so that they could replace the corresponding stars in a propagated version of the Hipparcos catalogue. It was necessary to propagate the HIP catalogue to the year 2015 since the TGAS catalogue provides the astrometry in the reference epoch J2015. In this way, we obtain a catalogue that is complete and has improved proper motions for the majority of the Hipparcos stars. Here we will assume both the catalogues to be complete for a magnitude of $V = 8.0$, thus allowing for the calculation of the local mass density. By the inclusion of Hipparcos stars with improved proper motions from the TGAS catalogue, a comparison between how well the TGAS catalogue works in relation to the HIP catalogue can hopefully be obtained.

4.2.1 Hipparcos 2015

This section will describe the Hipparcos sample where the positions of the stars were propagated to the year 2015 (the original HIP catalogue provides astrometry for the epoch J1991.25). For this HIP catalogue the positions of the stars were given in terms of right ascension and declination. In order to convert the positions from the equatorial coordinate system to the galactic one, the following equations were used

$$\sin(b) = \sin(\delta)\cos(i_g) - cos(\delta)\sin(\alpha - \alpha_N)\sin(i_g)$$

$$\cos(b)\cos(l - l_0) = \cos(\delta)\cos(\alpha - \alpha_N)$$

$$\cos(b)\sin(l - l_0) = \sin(\delta)\sin(i_g) + \cos(\delta)\sin(\alpha - \alpha_N)\cos(i_g)$$

where $i_g = 62.6°$, $\alpha_N = 282.25°$ and $l_0 = 33°$. The proper motions were also propagated from the equatorial coordinate system into the galactic coordinate system using the principles described in Poleski (2013). The values of the colour index $B - V$ for each star in the propagated HIP catalogue were originally not included. To resolve this, the colour index data from the original Hipparcos catalogue was manually cross-matched into the propagated catalogue.

4.2.2 Combined Sample

The combined sample contained Hipparcos stars from both the TGAS the propagated Hipparcos catalogues. The combined sample had 91 919 Hipparcos stars provided by the TGAS catalogue and an additional 26 036 from the original, propagated Hipparcos catalogue. The stars provided by the TGAS catalogue had improved proper motions, and could thus potentially give a more accurate estimation of the local mass density. The positions and proper motions for this catalogue were given in galactic coordinates. The colours used here were once again provided by the original Hipparcos catalogue and consisted of the V-magnitude and the B-V colour index.

4.3 Local Mass Density Estimate

In order to estimate the local mass density from eq. (22), values of the velocity dispersion in the z-direction, σ_w, and the tracer star density, $n(z)$, needs to be estimated. In section 4.1 it was mentioned that σ_w^2 needs to be constant for the entire stellar population if the local mass density is to be estimated by means of eq. (22). This is highly unlikely to be true for the two Hipparcos data catalogues used. To circumvent this issue, the complete samples will be divided into smaller sub-samples. For every sub-sample, a velocity dispersion σ_w can be estimated and held constant. As long as the sub-samples cover a small enough range in the colour index, the approximation regarding the constant value of σ_w should still provide a reasonable representation of the dispersion distribution, since the characteristics of main sequence stars are expected to be similar. Each of the sub-samples represent a number of stars that are spherically distributed in space around the Sun. The maximum radius of the sphere, r_{max} (in pc), will vary for each sub-sample as

$$r_{max} = \frac{1000}{(p_{min} + 1.5)} \tag{23}$$

Where the additional 1.5 mas is there to correct for the typical parallax uncertainties of the TGAS and Hipparcos catalogues. In order to obtain values of r_{max}, we must have values of p_{min}. However, we have neither r_{max} nor p_{min}, and we must instead resort to using the distance modulus in order to get values for the maximum radius for each sample

$$V - M_V = 5\log_{10}(r_{max}) + 5 = 5\log_{10}\left(\frac{1000}{p_{min} + 1.5}\right) + 5 \tag{24}$$

Where V is the Johnson V-magnitude and M_V is the absolute V magnitude. Since both the propagated Hipparcos catalogue as well as the combined sample only consist of Hipparcos stars, they can both be seen as complete to $V = 8.0$ magnitudes. We can thus hold $V = 8.0$

constant for each sample that we have defined, r_{max} will then correspond to the maximum distance that the samples are complete for, which is precisely what we wish to obtain. However, in order to solve eq. (24), values of $(M_V)_{max}$ are necessary for each sub-sample. By using the database YZVAR (see Bertelli et al. 2008 & Bertelli et al. 2009), theoretical Hertsprung-Russel diagrams showing isochrones for stars of solar composition could be produced. Figure 10 demonstrates the isochrones used and table 9 shows the properties of the H-R diagram in terms of the composition (Z & Y), the maximum age considered, $\log t_{max}$, and the difference in age between subsequent isochrones, $\log \Delta t$. Since each sample span across a certain colour region, a maximum value of the absolute V magnitude could be estimated using figure 10. This allows us to calculate values of both r_{max} and p_{min} for each individual sub-sample by using eq. (24).

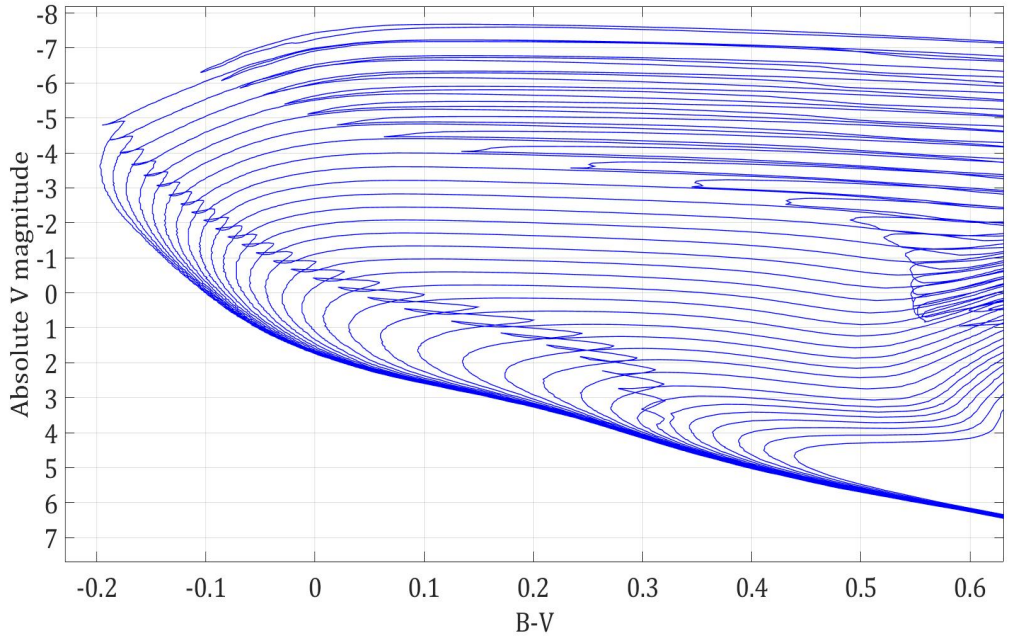

Figure 10: Theoretical isochrones of Solar composition were used to determine M_V.

Each sample is additionally divided into horizontal layers of thickness $\Delta z = 25$ pc, where all the stars per layer are calculated and divided by the layer volume. Figure 11 shows an illustration of how the sphere containing stars is divided into horizontal layers. In this way we obtain a value for the tracer star population density, $n(z)$, per layer. It is then possible to

Table 9:
Properties of the theoretical Hertsprung-Russel diagram.

Z	Y	$\log t_{max}$	$\log \Delta t$
0.0134	0.2485	10.3	0.1

plot the calculated values of $n(z)$ as a function of z. By fitting a parabola to this graph the curvature can be calculated. This parabola is given by

$$\ln n(z) = c_1 z^2 + c_2 z + c_3 \tag{25}$$

and from eq. (22) the curvature, Q, is given as the second partial derivative of $\ln n(z)$

$$Q = \frac{\partial^2 \ln n(z)}{\partial z^2} = 2c_1 \tag{26}$$

In this way, the local mass density can be estimated for each data sample and the average value of all the densities for the sub-samples correspond to the local mass density, ρ_0.

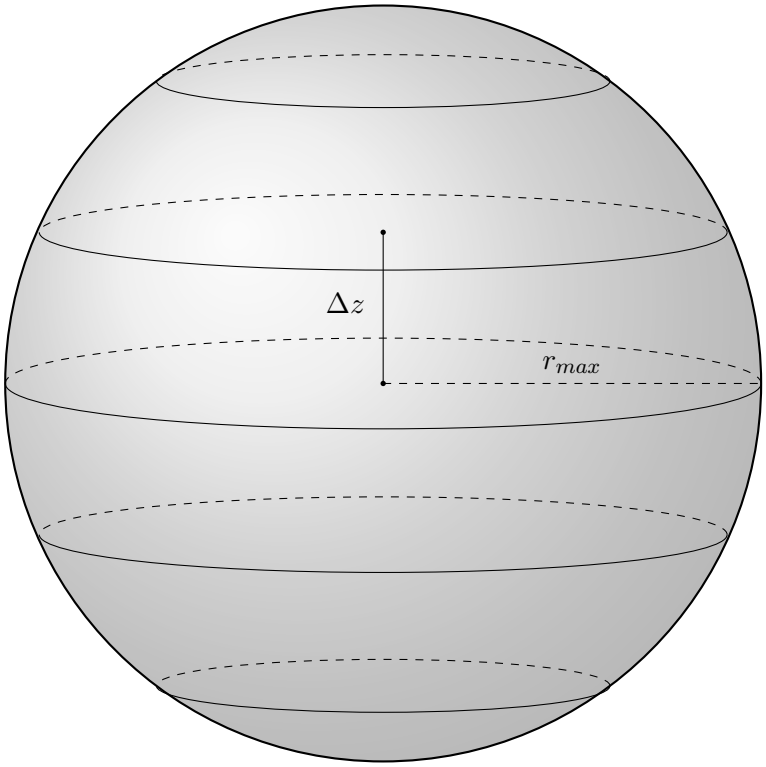

Figure 11: The data sub-samples represents a spherical distribution of stars where horizontal layers of thickness Δz are introduced.

4.3.1 Data Selection Criteria

In order to have the stars confined within a sphere with a radius corresponding to the maximum distance where catalogue completeness is still valid, we must have $p \geq p_{min}$. Both of the catalogues were divided into sub-samples in steps of 0.05 magnitudes of the colour index $B-V$ and the complete range was $-0.15 < B-V \leq 0.20$. Redder stars were not chosen due to them being older and thus having larger velocity dispersions. The stars in the respective samples should preferably all be members of the main sequence due to their similar characteristics making them more predictable. In addition, to assure that each sub-sample is representative of the population, the minimum number of stars per sample was set to be $N_{min} = 200$. If a sample did not contain that number of stars, the colour range for that particular sample was increased.

In section 4.2 the distance estimator used to obtain r_{max} from a parallax measurement was given by eq. (23). However, according to Bailer-Jones (2015, 2016a, 2016b), in order to use such an inverse-parallax distance estimator, the fractional parallax error (FPE) must not be larger than 0.2. If the FPE is larger than this set value, the relationship between distances and parallaxes becomes increasingly more complex. In addition, in order to assure that high quality data is used in the calculation of the local mass density, a low FPE is necessary. However, if a value of the FPE that is much lower than 0.2 is selected, many stars from the catalogues will be discarded. There must exist a balance between the statistical aspect and the quality aspect of the study. By setting the maximum FPE to be 0.2, we can be certain that the distance estimator used is working as intended while simultaneously using the largest possible fraction of the respective catalogue. Table 10 shows a summary of the selection rules for the sub-samples that were applied to both the catalogues containing Hipparcos stars.

Table 10:
SELECTION CRITERIA FOR BOTH CATALOGUES.

V_{max} [mag]	parallax, p [mas]	FPE, σ_p/p	N_{min}	$C_1 < B-V \leq C_2$
				$C_1 - C_2 = 0.05$
≤ 8.0	$\geq p_{min}$	≤ 0.2	200	$(C_1)_{min} = -0.15$
				$(C_2)_{max} = 0.2$

4.4 Results

4.4.1 Dispersion

Table 11 and 12 shows the velocity dispersions for the different sub-samples of the propagated Hipparcos catalogue and the combined sample respectively.

Table 11:
DISPERSIONS FOR PROPAGATED HIP CATALOGUE SUB-SAMPLES.

Sub-Sample	σ_w, [km/s]
$-0.15 < B-V \leq -0.1$	5.68
$-0.10 < B-V \leq -0.05$	4.95
$-0.05 < B-V \leq 0.0$	6.14
$0.0 < B-V \leq 0.05$	6.09
$0.05 < B-V \leq 0.10$	6.25
$0.10 < B-V \leq 0.15$	6.81
$0.15 < B-V \leq 0.20$	8.47

Figure 12 and 13 shows σ_u^2 (red line), σ_v^2 (blue line), σ_w^2 (black line) as a function of $B-V$ for the propagated Hipparcos catalogue and the combined sample respectively. It is evident from these figures that σ_w^2 does increase for older, redder stars. However, the ranges in the colour index $B-V$ that we chose to use do not seem to have been affected by the increased dispersions for older stars dramatically since the increase in σ_w^2 for higher $B-V$ values is fairly smooth. This is a good indication that the stars used here should be able to give consistent results of the local mass density.

Table 12:
SUB-SAMPLE DISPERSIONS FOR THE COMBINED SAMPLE.

Sub-Sample	σ_w, [km/s]
$-0.15 < B-V \leq -0.1$	5.79
$-0.10 < B-V \leq -0.05$	5.12
$-0.05 < B-V \leq 0.0$	5.21
$0.0 < B-V \leq 0.05$	6.23
$0.05 < B-V \leq 0.10$	6.10
$0.10 < B-V \leq 0.15$	6.80
$0.15 < B-V \leq 0.20$	8.18

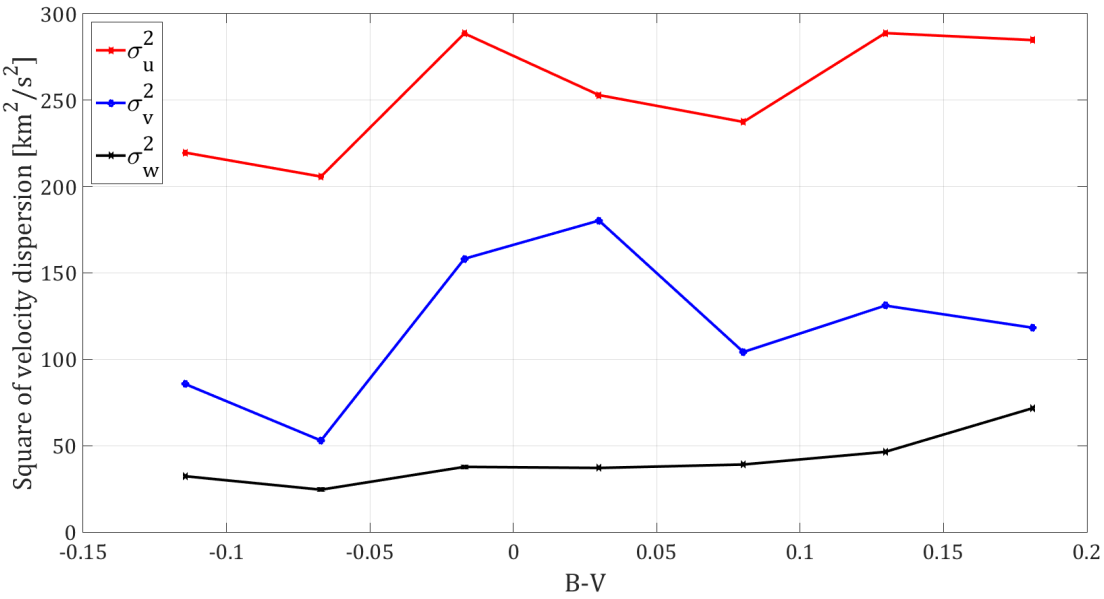

Figure 12: DISPERSION AS A FUNCTION OF COLOUR INDEX FOR HIP2015.

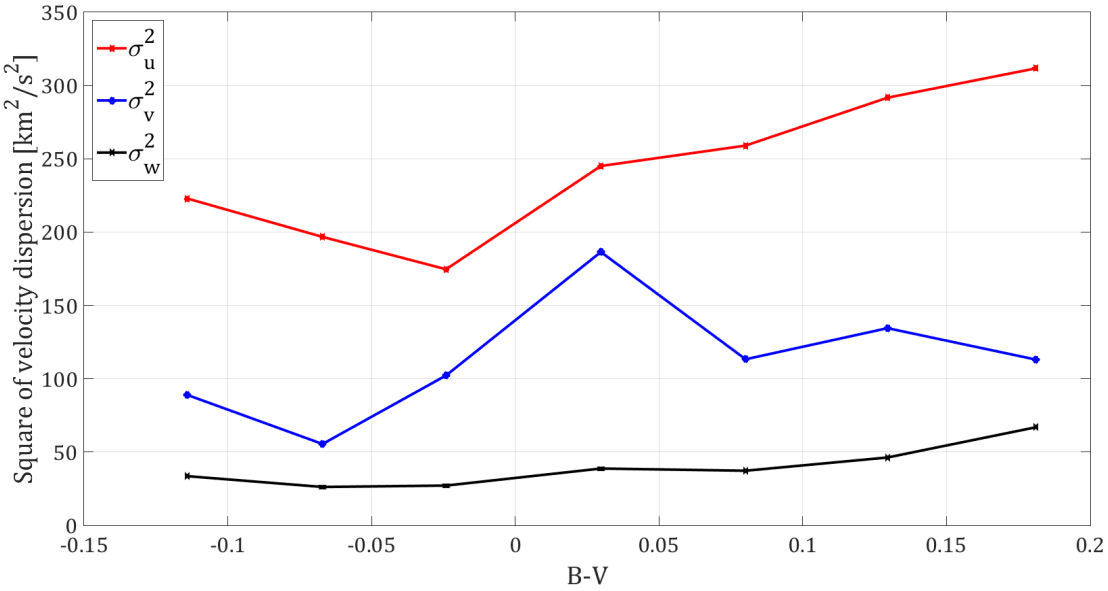

Figure 13: Dispersion as a function of colour index for the combined sample.

4.4.2 Local Mass Density

Table 12 summarizes the calculated values of ρ_0 for both the propagated Hipparcos 2015 catalogue and the combined Sample.

Table 13:
Local mass density in $M_\odot$ pc^{-3} calculated from the catalogues.

	HIP2015	Combined Sample
ρ_0	0.112 ± 0.009	0.113 ± 0.006

Figure 14 and 15 shows the estimated values of ρ_0 for each of the smaller sub-samples for the propagated and combined Hipparcos catalogues respectively. It is apparent that the combined sample that includes stars from the TGAS catalogue does not provide a significant difference compared to the propagated Hipparcos catalogue other than it being slightly more smooth and consistent. This reduction of outliers for the mass density graph of the combined sample is most likely due to the improved proper motions from the TGAS catalogue. The values of ρ_0 presented in table 12 as well as the characteristics of the graphs in figures 14 and 15 are very similar to each other, implying that the combined sample is equal in performance to the Hipparcos catalogue when it comes to the dynamical estimate of the mass density.

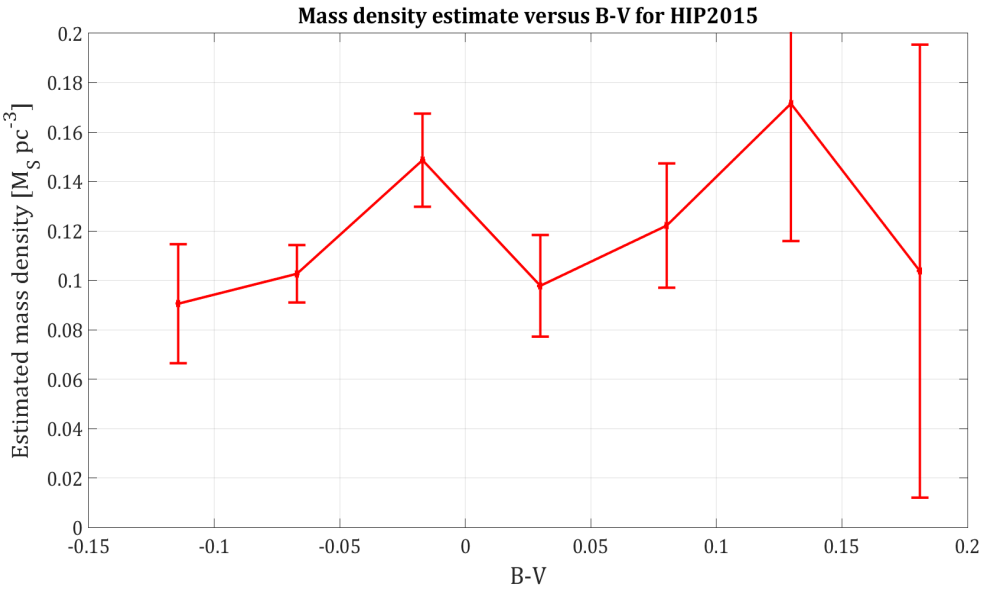

Figure 14: Sub-sample estimation of local mass ensity for HIP2015.

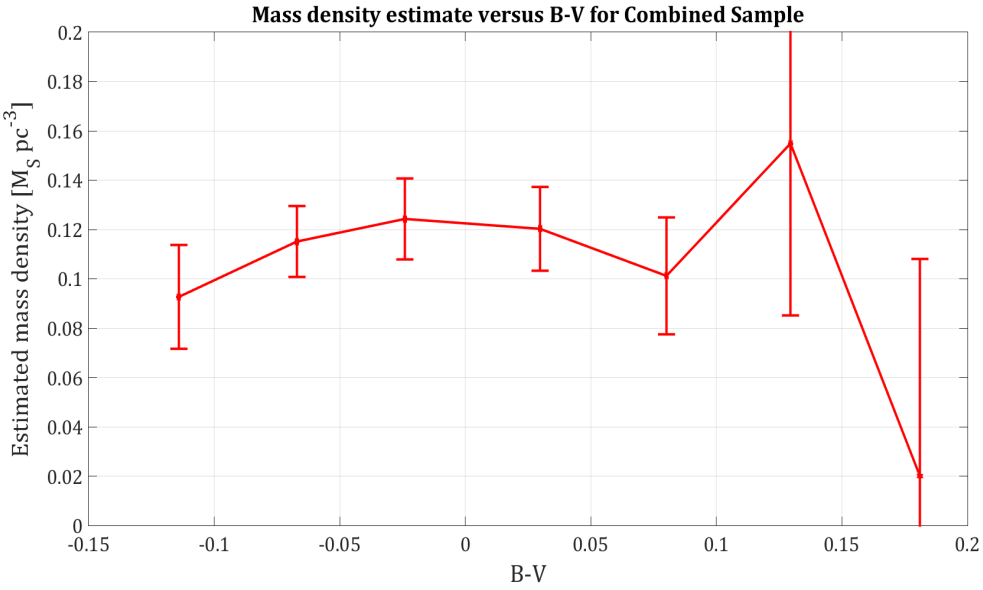

Figure 15: Sub-sample estimates of ρ_0 for the combined sample.

4.5 Conclusion

From the results presented in table 13 and figures 14-15, it can be concluded that the TGAS catalogue performs almost identically when compared to the propagated Hipparcos catalogue. The results presented here are in fairly good agreement with those presented by Crézé et al. (1998) and Holmberg & Flynn (2000). However, it should be mentioned that the creation of the combined sample was not so simple and included multiple cross-matches. Mixing and matching of catalogues in this way is prone to introducing an increase in the formal errors for the end catalogue as a whole. Even though the combined sample did provide with results that were nearly identical with the results from the propagated Hipparcos catalogue, it is still recommended that the TGAS catalogue is avoided when dynamically estimating the local mass density. The recommendation is to instead use the Hipparcos stars from the original catalogue. Hopefully when Gaia-DR2 is released it will be possible to dynamically estimate the local mass density without needing to first create a catalogue such as TGAS to compensate for the shortcomings of the release. In this way, it would be possible to give an estimate regarding the performance of the complete Gaia catalogue.

Acknowledgements

I would like to express my gratitude towards my family for always supporting me when I was in need of guidance and advice.

I also wish to thank my supervisor D. Hobbs for providing me with not only advice, discussion and answers to questions, but also what questions need be asked in order to construct this Bachelor's thesis successfully.

Lastly, I wish to thank all my friends who have supported me during my time writing this thesis. In particular I would like to express my appreciation towards S. Samadi that always kept me company in school during my studies.

Appendices

A Oort constant estimation, Supplementary figures

In this appendix, additional figures describing data from section 3 are presented.

A.1 Hipparcos Figures

Figures 16-18 shows the proper motion in galactic longitude as a function of l for the three samples that were obtained from the propagated Hipparcos catalogue.

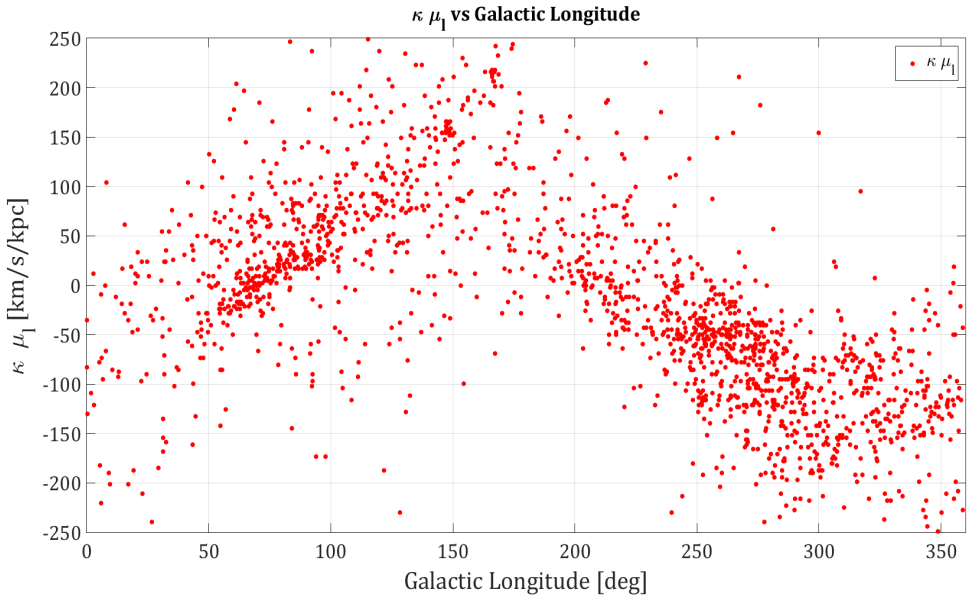

Figure 16: μ_l VS. l FOR FIRST HIPPARCOS SAMPLE. $B-V$ RANGE: $-0.15 < B-V \leq 0.0$.

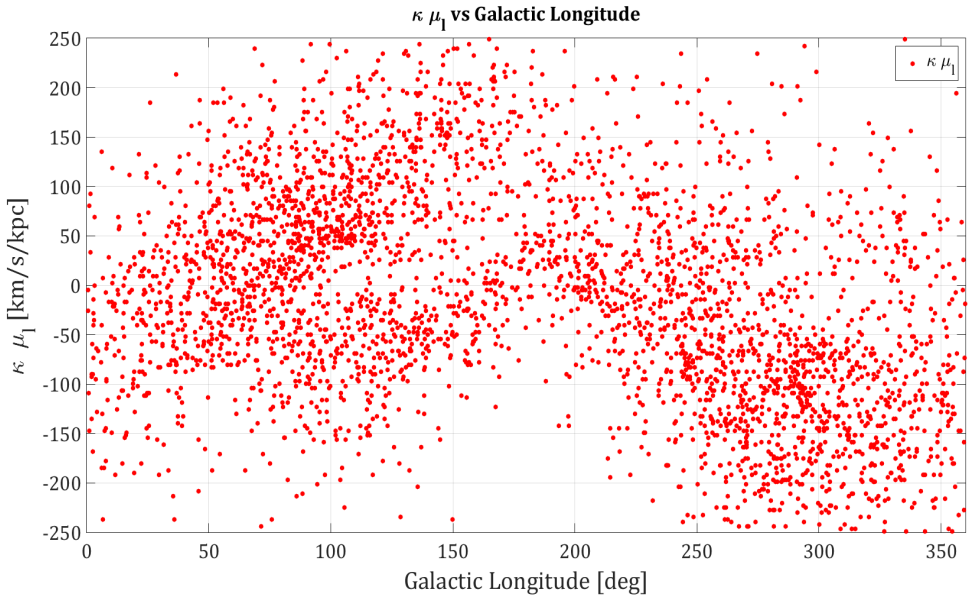

Figure 17: μ_l VS. l FOR SECOND HIPPARCOS SAMPLE. $B-V$ RANGE: $0.0 < B-V \leq 0.2$.

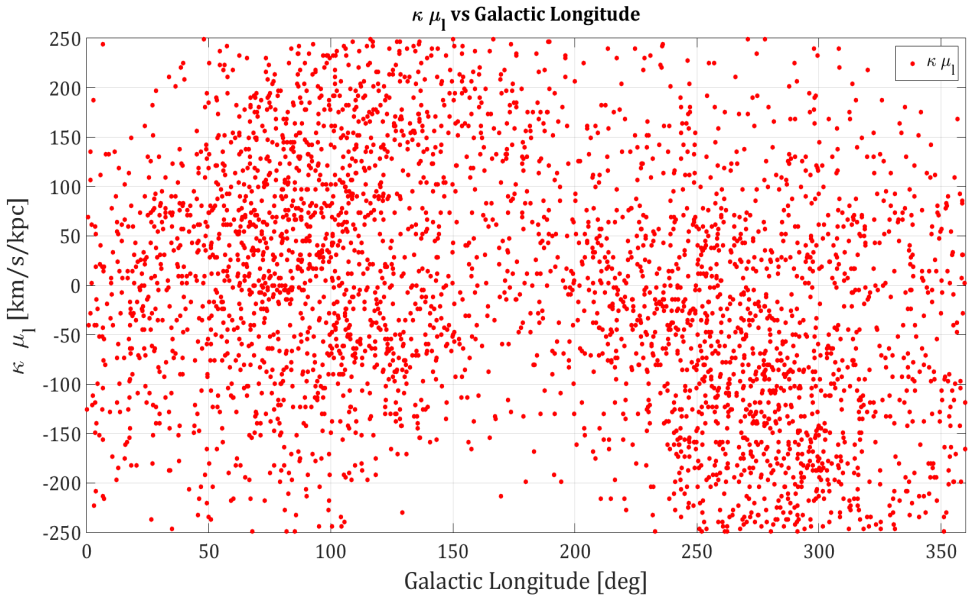

Figure 18: μ_l VS. l FOR LAST HIPPARCOS SAMPLE. $B-V$ RANGE: $0.2 < B-V \leq 0.4$.

Figures 19-21 instead show the proper motion in galactic latitude as a function of b for the three samples obtained from the Hipparcos catalogue. Note that the range in latitude is $-20 \leq b \leq 20$.

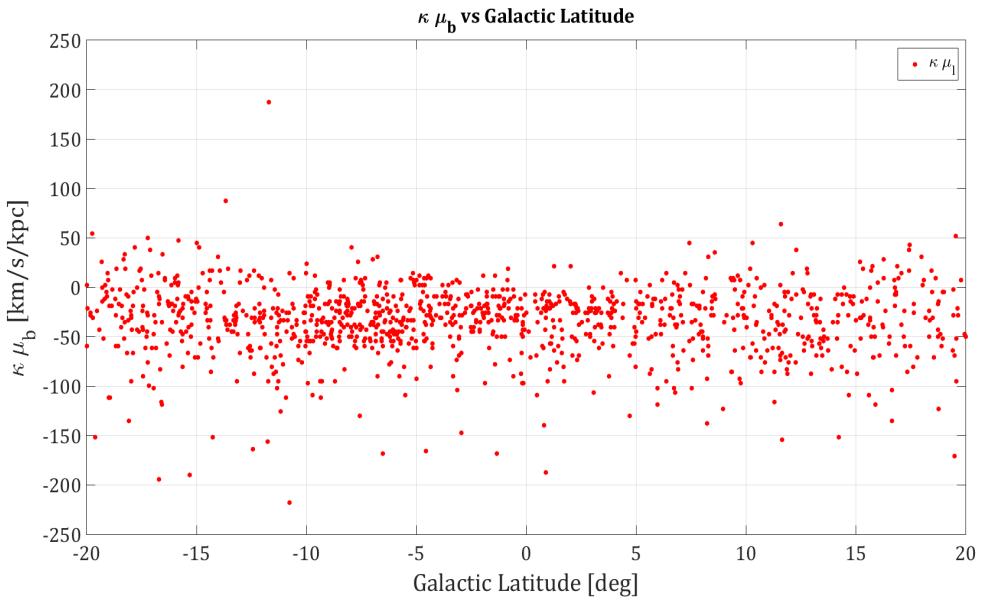

Figure 19: μ_b VS. b FOR FIRST HIPPARCOS SAMPLE. $B-V$ RANGE: $-0.15 < B-V \leq 0.0$.

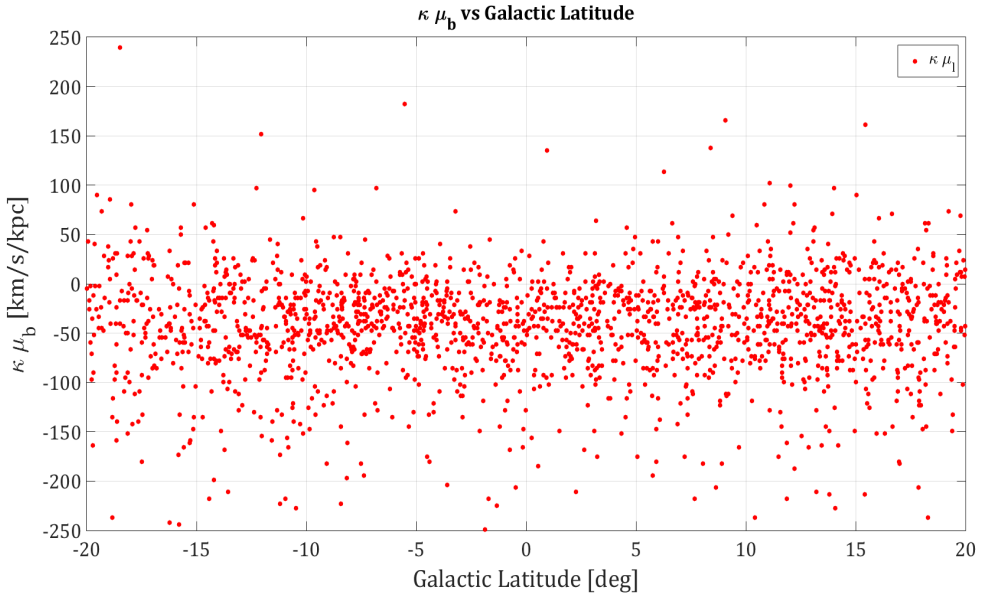

Figure 20: μ_b VS. b FOR SECOND HIPPARCOS SAMPLE. $B-V$ RANGE: $0.0 < B-V \leq 0.2$.

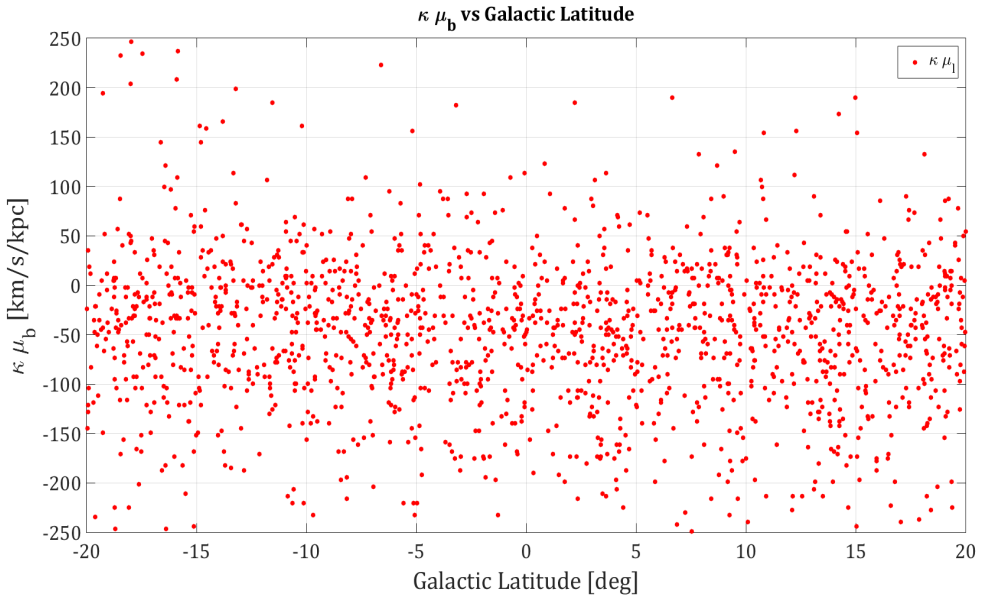

Figure 21: μ_b VS. b FOR THIRD HIPPARCOS SAMPLE. $B-V$ RANGE: $0.2 < B-V \leq 0.4$.

A.2 TGAS Figures

Figures 22-24 show the proper motions of the stars in the cross-match as a function of the galactic latitude for all three samples respectively.

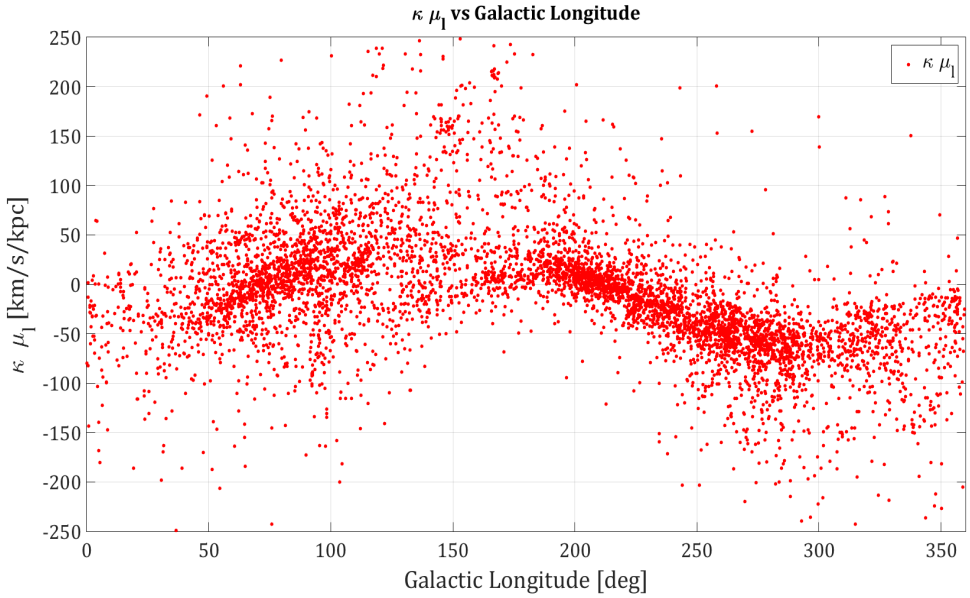

Figure 22: μ_l VS l FOR THE FIRST MATCHED SAMPLE. RANGE IN COLOUR INDEX: $-0.15 < J - K_s \leq 0.0$.

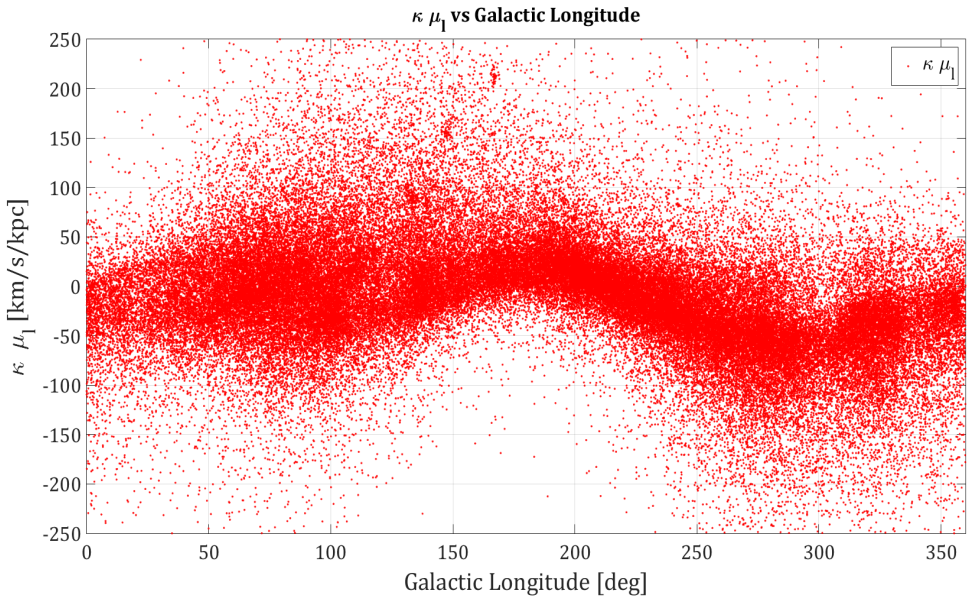

Figure 23: μ_l VS l FOR THE SECOND MATCHED SAMPLE. RANGE IN COLOUR INDEX: $0.0 < J - K_s \leq 0.2$.

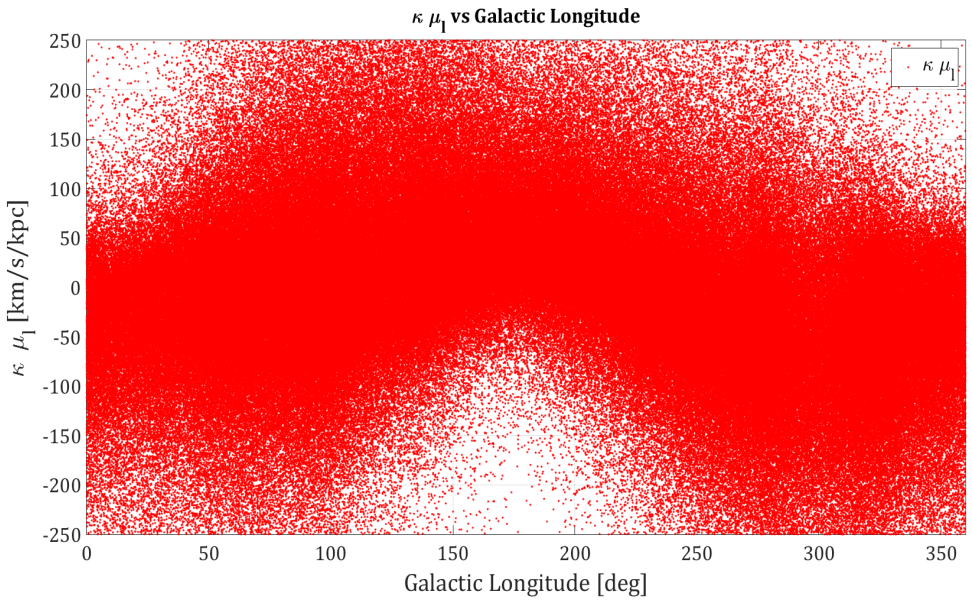

Figure 24: μ_l VS l FOR THE THIRD MATCHED SAMPLE. RANGE IN COLOUR INDEX: $0.2 < J - K_s \leq 0.4$.

Figures 25-27 shows the relation between the proper motion in b and the galactic latitude.

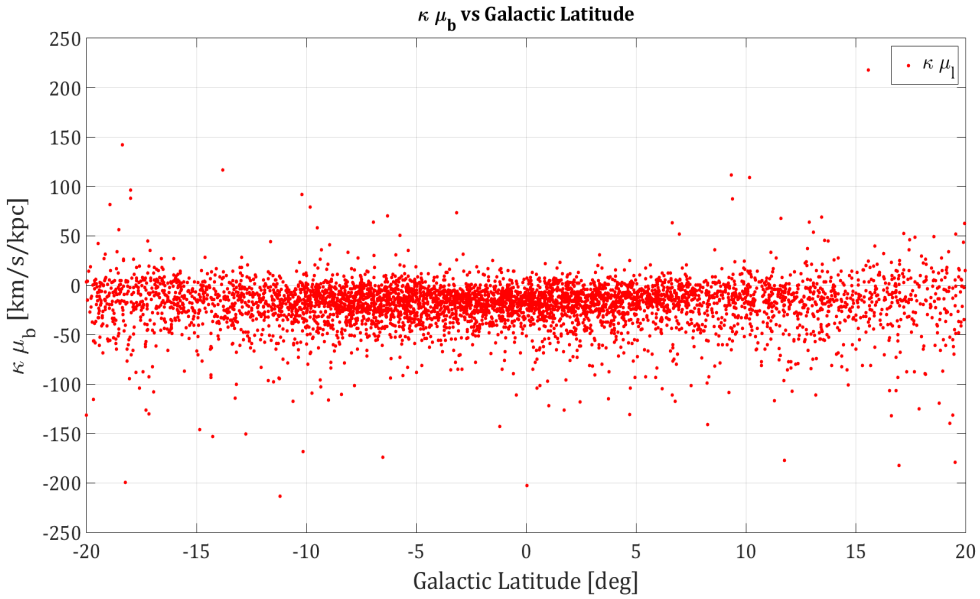

Figure 25: μ_b VS b FOR THE FIRST MATCHED SAMPLE. RANGE IN COLOUR INDEX: $-0.15 < J - K_s \leq 0.0$.

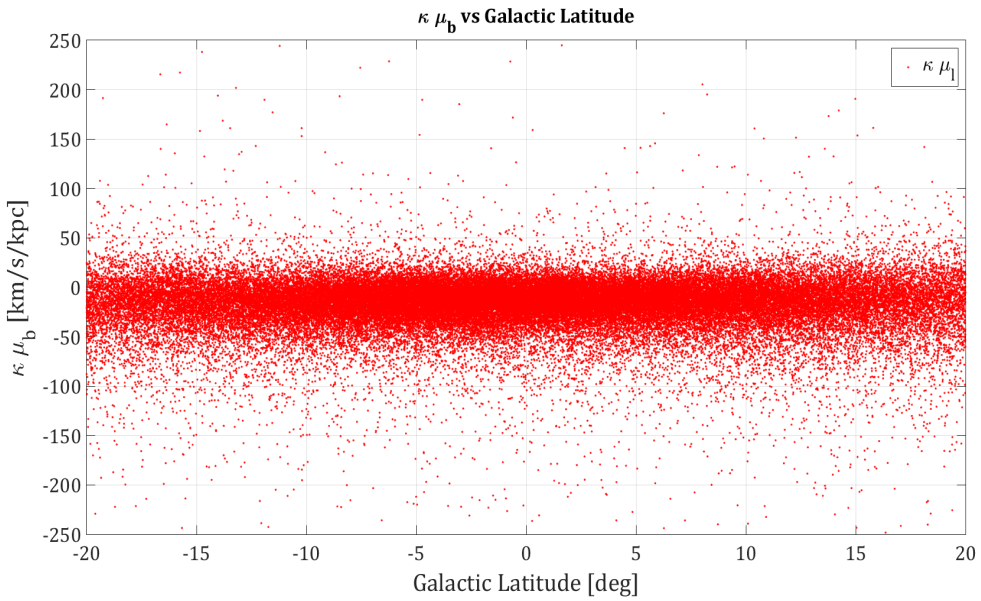

Figure 26: μ_b VS b FOR THE SECOND MATCHED SAMPLE. RANGE IN COLOUR INDEX: $0.0 < J - K_s \leq 0.2$.

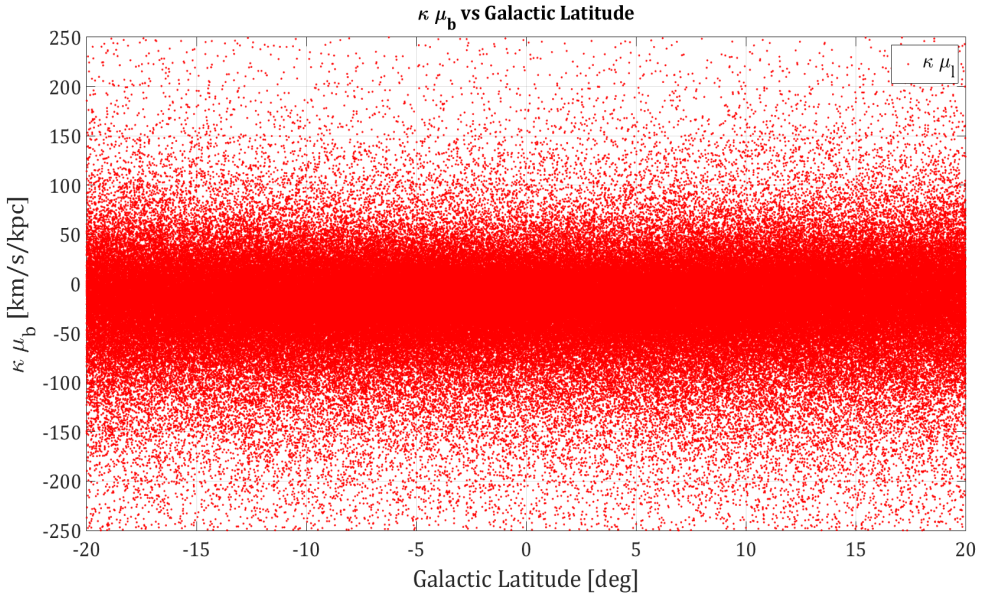

Figure 27: μ_b VS b FOR THE THIRD MATCHED SAMPLE. RANGE IN COLOUR INDEX: $0.2 < J - K_s \leq 0.4$.

B The Dispersion Matrix

In this appendix the details surrounding the estimation of the dispersion matrix $\boldsymbol{D}$ are shown. This derivation was originally documented by Lennart Lindegren in the instruction manual for the project *P2: The motions of nearby stars and the LSR* that worked as a part of the course **ASTM13 - Dynamical Astronomy** held at Lund University. In this derivation, a subscript i refers to properties of a star i in an arbitrary data sample.

Values for the velocity dispersion in the x, y and z-directions can be obtained from the dispersion matrix

$$\boldsymbol{D} = \begin{bmatrix} D_{11} & D_{12} & D_{13} \\ D_{21} & D_{22} & D_{23} \\ D_{31} & D_{32} & D_{33} \end{bmatrix} \tag{A.1}$$

where

$$D_{11} = \sigma_u^2, \quad D_{22} = \sigma_v^2, \quad D_{33} = \sigma_w^2 \tag{A.2}$$

In principle, the dispersion matrix can be estimated using the sample average

$$\boldsymbol{D} = \frac{1}{N} \sum_{i=1}^{N} \Delta \boldsymbol{v}_i \Delta \boldsymbol{v}_i^T \tag{A.3}$$

Where $\Delta \boldsymbol{v}_i$ is

$$\Delta \boldsymbol{v}_i = \boldsymbol{v}_i - \langle \boldsymbol{v} \rangle \tag{A.4}$$

and is here called the peculiar velocity, describing how much the velocity, $\boldsymbol{v}_i$, of a star in a data sample deviates from the average velocity of the same sample, $\langle \boldsymbol{v} \rangle$.

In order to calculate the space velocity of any star, the position (l, b), parallax (p), proper motions (μ_l, μ_b) and the radial velocity v_r are needed

$$\boldsymbol{v_i} = \boldsymbol{l}_i \frac{K(\mu_l)_i}{p_i} + \boldsymbol{b}_i \frac{K(\mu_b)_i}{p_i} + \boldsymbol{u}_i (v_r)_i \tag{A.5}$$

where $K = 4.7405$ and $(\boldsymbol{l}_i, \boldsymbol{b}_i, \boldsymbol{u}_i)$ correspond to the normal triad vectors

$$\boldsymbol{u}_i = \begin{bmatrix} \cos b_i \cos l_i \\ \cos b_i \sin l_i \\ \sin b_i \end{bmatrix} \quad \boldsymbol{l}_i = \begin{bmatrix} -\sin l_i \\ \cos l_i \\ 0 \end{bmatrix} \quad \boldsymbol{b}_i = \begin{bmatrix} -\sin b_i \cos l_i \\ -\sin b_i \sin l_i \\ \cos b_i \end{bmatrix} \tag{A.6}$$

However, the TGAS nor Hipparcos provide radial velocities for stars and instead we are inevitably restricted to working with the tangential velocity vector $\boldsymbol{\tau}_i$. This vector is related to the space velocity as

$$\boldsymbol{\tau}_i = \boldsymbol{T}_i \boldsymbol{v}_i \tag{A.7}$$

Where $\boldsymbol{T}_i$ is the tangential projection matrix

$$\boldsymbol{T}_i = \boldsymbol{I} - \boldsymbol{u}_i \boldsymbol{u}_i^T \tag{A.8}$$

$\boldsymbol{I}$ is the 3×3 identity matrix. The tangential projection matrix projects the space velocity $\boldsymbol{v}_i$ on the tangent plane and thus gives an expression for $\boldsymbol{\tau}_i$. Note that $\boldsymbol{T}_i$ is a singular matrix and thus eq. (A.7) cannot be used directly to obtain $\boldsymbol{v}_i$. However, by using the principles described in Dehnen & Binney (1998) we can obtain the mean velocity using eq. (A.7) as

$$\langle \boldsymbol{v} \rangle = \langle \boldsymbol{T} \rangle^{-1} \langle \boldsymbol{\tau} \rangle \tag{A.9}$$

It is evident from eq. (A.9) that by only considering $\langle \boldsymbol{T} \rangle$ and $\langle \boldsymbol{\tau} \rangle$ we can estimate $\langle \boldsymbol{v} \rangle$. Furthermore, we introduce the tangential peculiar velocity

$$\Delta \boldsymbol{\tau}_i = \boldsymbol{T}_i \Delta \boldsymbol{v}_i = \boldsymbol{\tau}_i - \boldsymbol{T}_i \langle \boldsymbol{v} \rangle \tag{A.10}$$

Where we used eq. (A.4) to evaluate $\Delta \boldsymbol{v}_i$. We also introduce the 3×3 matrix $\boldsymbol{B}$

$$\boldsymbol{B} = \left\langle \Delta \boldsymbol{\tau} \Delta \boldsymbol{\tau}^T \right\rangle = \frac{1}{N} \sum_{i=1}^{N} \Delta \boldsymbol{\tau}_i \Delta \boldsymbol{\tau}_i^T \tag{A.11}$$

In a similar way that we could estimate $\langle \boldsymbol{v} \rangle$ from $\langle \boldsymbol{\tau} \rangle$, we can estimate $\boldsymbol{D}$ from $\boldsymbol{B}$.
In what is to follow, we will omit the subscript i from each mathematical expression for clarity. We start of by rewriting the expression for the tangential peculiar velocity from eq. (A.10) in component form

$$\Delta \tau_k = \sum_{m=1}^{3} T_{km} \Delta v_m \tag{A.12}$$

where $k = m = 1, ..., 3$. We will implement the Einstein summation convention for brevity meaning $\Delta \tau_k = T_{km} \Delta v_m$ is equivalent to eq. (A.12). Combining eqs. (A.11) and (A.12) we can write the components of $\boldsymbol{B}$ as

$$B_{kl} = \langle \Delta \tau_k \Delta \tau_l \rangle = \langle T_{km} \Delta v_m T_{ln} \Delta v_n \rangle \tag{A.13}$$

Where $l = n = 1, ..., 3$. By assuming statistical independence between the tangential projection matrix and the peculiar motion we obtain

$$B_{kl} = \langle T_{km} T_{ln} \rangle \langle \Delta v_m \Delta v_n \rangle = \langle T_{km} T_{ln} \rangle D_{mn} \tag{A.14}$$

In order to solve eq. (A.14) we introduce the following vectors

$$\boldsymbol{b} = \begin{bmatrix} B_{11} \\ B_{12} \\ B_{13} \\ B_{22} \\ B_{23} \\ B_{33} \end{bmatrix}, \quad \boldsymbol{d} = \begin{bmatrix} D_{11} \\ D_{12} \\ D_{13} \\ D_{22} \\ D_{23} \\ D_{33} \end{bmatrix} \tag{A.15}$$

$$A = \begin{bmatrix} 11.11 & (11.12 + 12.11) & (11.13 + 13.11) & 12.12 & (12.13 + 13.12) & 13.13 \\ 11.21 & (11.22 + 12.21) & (11.23 + 13.21) & 12.22 & (12.23 + 13.22) & 13.23 \\ 11.31 & (11.32 + 12.31) & (11.33 + 13.31) & 12.32 & (12.33 + 13.32) & 13.33 \\ 21.21 & (21.22 + 22.21) & (21.23 + 23.21) & 22.22 & (22.23 + 23.22) & 23.23 \\ 21.31 & (21.32 + 22.31) & (21.33 + 23.31) & 22.32 & (22.33 + 23.32) & 23.33 \\ 31.31 & (31.32 + 32.31) & (31.33 + 33.31) & 32.32 & (32.33 + 33.32) & 33.33 \end{bmatrix} \tag{A.16}$$

Each element in $\boldsymbol{A}$ corresponds to the numbers $km.ln$ that $T_{km}T_{ln}$ will have. By looking at the equation

$$\boldsymbol{b} = \boldsymbol{A}\boldsymbol{d} \tag{A.17}$$

The components from the dispersion matrix that are of interest can be obtained as $\boldsymbol{d} = \boldsymbol{A}^{-1}\boldsymbol{b}$.

List of Figures

List of Tables

References

Bahcall, J. N., Beichman, C. A, Canizares, C., et al. 1991, The Decade of Discovery in Astronomy and Astrophysics, A & A Committee, Washington D.C.
Bailer-Jones, C. A. L., 2015, Publ. Astron. Soc. Pac., 127, 956
Bailer-Jones, C. A. L., 2016a, ApJ, 832, 2
Bailer-Jones, C. A. L., 2016b, ApJ, 833, 1
Bertelli, G., Girardi, L., Marigo, P., et al. 2008, A&A 484, 815–830
Bertelli, G., Girardi, L., Marigo, P., et al. 2009, A&A 508, 355–369
Bobylev, V. V., Bajkova, A. T., 2017, Astron. Lett, 43, 3
Boch, T., Pineau, F. X., Derriere, S., 2016, CDS xMatch service documentation
Bovy, J., 2016, MNRAS, 468, 1, L63-L67
Casagrande, L., Schönrich, R., Asplund, M., et al. 2011, A&A 530, A138
Chandrasekhar, S., 1960, Principles of Stellar Dynamics, Dover Publications, New York
Crézé, M., Chereul, M., Bienaymé, O., et al. 1997, A&A, 329, 920–936
Cutri, R. M., Skrutskie, M. F., Van Dyk, S. et al., 2003, Explanatory Supplement to the 2MASS All Sky Data Release and Extended Mission Products
Dehnen, W., Binney, J. J., 1998, MNRAS, 298, 387–394
Gaia Collaboration, et al., 2017, A&A, 601, A19
Gaia Collaboration, et al.: The Gaia Mission, 2016, A& A 595, A2
Gaia Collaboration, et al.: Gaia Data Release 1, 2016, A&A 595, A1
Høg, E., Fabricius, C., Makarov, V. V., et al., 2000, A&A, 355, L27–L30
Holmberg, J., Flynn, C., 2000, Mon. Not. R. Astron. Soc. 313, 209-216
Kapteyn, J. C., Van Rhijn, P. J., 1920, ApJ, 52, 23
Kapteyn, J. C., 1922, ApJ, 55, 302
Kerr, F. J., Lynden-Bell, D., 1986, MNRAS, 221, 1023-1038
Lindegren, L., 2014, Dynamical astronomy - Lecture notes for ASTM13
Lindegren, L., Lammers, U., Hobbs, D., et al. 2012, A&A 538, A78
Michalik, D., Lindegren, L., Hobbs, D., 2015, A&A 574, A115
Michalik, D., Lindegren, L., Hobbs, D., et al. 2014, A&A 571, A85
Ogrodnikoff, K., 1932, Zeitschrift für Astrophysik, Vol. 4, p.190
Olling,. R. P., Dehnen, W., 2003, ApJ 599, 275-296
Oort, J. F., 1927, Bull. Astr. Inst. Neth., 3, 275
Oort, J. F., 1932, Bull. Astr. Inst. Neth., 6, 249
Perryman, M. A. C., 2008, Astronomical Applications of Astrometry. Cambridge University Press, Cambridge
Perryman, M. A. C., Hassan, H., 1989, ESA Bulletin 58
Perryman, M. A. C., Lindegren, L., Kovalevsky, J., 1997, A&A, 323, L49-L51
Perryman, M. A. C., de Boer, K. S., Gilmore, G., 2001, A&A 369, 339-363
Poleski, R., 2013, arXiv:1306.2945
Schönrich, R., Binney, J., Dehnen, W., 2009, MNRAS, 403, 1829–1833
Skrutskie, M. F., Cutri, R. M., Stiening, R., et al. 2006, AJ, 131, 1163-1183